

A simplified 3-D Navier-Stokes numerical model for landslide-tsunami: Application to the Gulf of Mexico

J. Horrillo,¹ A. Wood,¹ G.-B Kim,¹ and A. Parambath¹

Received 10 December 2012; revised 21 October 2013; accepted 26 November 2013; published 17 December 2013.

[1] A simplified three-dimensional Navier-Stokes (3-D NS) model for two fluids, water and landslide material (mudslide) is presented and validated with standard laboratory experiments. Dubbed TSUNAMI3D (Tsunami Solution Using Navier-Stokes Algorithm with Multiple Interfaces) is applied to a 3-D full-scale landslide scenario in the Gulf of Mexico (GOM), i.e., the East-Breaks underwater landslide. The simplified 3-D NS model is conceived to be computationally efficient for tsunami calculations. The simplification is derived from the large aspect ratio of the tsunami waves (wavelength/wave-height) and the selected computational grid that has a smaller aspect ratio. This allows us to assume a horizontal fluid surface in each individual cell containing the interface (air-water, air-mudslide, and water-mudslide). The tracking of fluid interfaces is based on the Volume of Fluid method and the surfaces are obtained by integrating the fluxes of each individual fluid cell along the water column. In the momentum equation, the pressure term is split into two components, hydrostatic and nonhydrostatic. The internal friction is solved in a simplified manner by adjusting the viscosity coefficient. Despite the simplification to get an efficient solution, the numerical results agree fairly well with standard landslide laboratory experiments required by the National Tsunami Hazard Mitigation Program for tsunami model validation. The numerical effect caused by using a sharp versus a diffusive water-mudslide interface for a full-scale landslide-tsunami scenario is also investigated. Observations from this experiment indicated that choosing a sharp or diffusive interface seems to have no remarkable effect at early stages of the tsunami wave propagation. Last, a large scale 3-D numerical simulation is carried out for the ancient GOM's East-Breaks landslide by using the simplified model to calculate the early stages of the tsunami wave propagation.

Citation: Horrillo, J., A. Wood, G.-B Kim, and A. Parambath (2013), A simplified 3-D Navier-Stokes numerical model for landslide-tsunami: Application to the Gulf of Mexico, *J. Geophys. Res. Oceans*, 118, 6934–6950, doi:10.1002/2012JC008689.

1. Introduction

[2] Recent assessments of tsunami hazards along the Gulf of Mexico (GOM) carried out by the U.S. Geological Survey (USGS) and the National Tsunami Hazard Mitigation Program (NTHMP) have identified underwater landslides as the primary potential source of tsunami generation [ten Brink *et al.*, 2009; Horrillo *et al.*, 2010]. Tsunami generation by underwater landslides depends on the geological characteristic of the slope materials and the triggering mechanism affecting the continental shelf. Common mechanisms to initiate an underwater landslide and the ensuing tsunami are: (a) earthquakes, (b) overpressure due to rapid

deposition of soil sediments, (c) presence of weak soil layers, (d) wave loading on sea-bottom by storms or hurricanes, (e) build up of the excess pore water pressure, (f) gas hydrate dissociation by change of temperature or pressure, (g) groundwater seepage, and (h) slope oversteepening [Hampton and Locat, 1996; Locat and Lee, 2002; Mason *et al.*, 2006]. Although a massive underwater landslide in the GOM is considered a potential hazard, the probability of such an event is quite low [Dunbar and Weaver, 2008]. The probability of occurrence is related to large ancient landslides which were probably active prior to 7000 years ago when large quantities of sediments were emptied into the GOM [ten Brink *et al.*, 2009]. However, nowadays sediments continue to empty into the GOM mainly from the Mississippi river. The sediment supply contributes to slope steepening and also to the increasing of the excess pore water pressure in the underlying soils, which may lead to further landslide activities. Recent evidence from seismic records of small-scale energetic seismic-waves in the GOM have confirmed that there is a probability of recurrence [Dellinger and Blum, 2009].

¹Maritime Systems Engineering, Texas A&M University at Galveston, Texas, USA.

Corresponding author: J. Horrillo, Maritime Systems Engineering, Texas A&M University at Galveston, 200 Seawolf Park, P.O. Box 1675, Galveston, TX 77553, USA. (horrillj@tamug.edu)

[3] In the past century, the seriousness of this threat became evident after the 1929 Grand Banks underwater landslide event, which produced tsunami waves of 3–8 m high, killing 28 people along the Newfoundland coastline [Cranford, 2000; Clague *et al.*, 2003]. Attempts to uncover the underlying physics came initially by a hand full of laboratory experiments [Wiegel, 1955; Law and Brebner, 1968; Heinrich, 1992; Watts, 1997]. These experiments used simple solid boxes sliding down incline planes. Further insight into the phenomenon was achieved with 2-D and 3-D experiments involving granular slide material on very steep slopes (fjord-like slopes) [Huber, 1980, 1982]. However, it was not until after the 1998 Papua New Guinea (PNG) tsunami that a thorough investigation of the underwater slide mechanisms and the generated tsunami was carried out in detail. This event claimed at least 2200 lives when waves up to 15 m high flooded the country's northern coast; this has been widely documented in e.g., Tanioka and Ruff [1998], Kikuchi *et al.* [1998], Tanioka [1999], Sweet *et al.* [1999], Tappin *et al.* [1999], Kawata *et al.* [1999], Geist [2000], Heinrich *et al.* [2000], Tappin *et al.* [2001], Imamura and Hashi [2002], Synolakis *et al.* [2002], Satake and Tanioka [2003], and it has served as the prelude for advanced landslide-tsunami investigations. However, the field data obtained from landslide-tsunami events are still very limited, so modelers depend heavily on laboratory experiments and analytical solutions for their research studies and numerical model validations. Other events of interest to the tsunami research community are the massive subaerial rockfall into Gilbert Inlet at the head of Lituya Bay, triggered by the earthquake on July, 1958, and the most recent landslide-tsunami occurred in the aftermath of Haiti earthquake on January, 2010 [Fritz *et al.*, 2009, 2013].

[4] Recent landslide laboratory experiments [e.g., Fritz, 2002; Grilli and Watts, 2005; Liu *et al.*, 2005; Enet and Grilli, 2005, 2007], produced a variety of empirical formulations [e.g., Watts, 1998, 2000; Enet *et al.*, 2003; Synolakis and Raichlen, 2003; Raichlen and Synolakis, 2003; Fritz *et al.*, 2004; Lynett and Liu, 2005; Heller, 2007; Heller and Hager, 2010], that together with several 1-D analytical solutions [e.g., Noda, 1970; Hunt, 1988; Tinti and Bortolucci, 2000; Tinti *et al.*, 2001; Okal and Synolakis, 2003; Liu *et al.*, 2003; Pelinovsky, 2003; Haugen *et al.*, 2005; Didenkulova *et al.*, 2010] and 2-D and 3-D analytical solutions [e.g., Novikova and Ostrovsky, 1978; Pelinovsky and Poplavsky, 1997; Ward, 2001] have proved to be essential in continuing developing, verifying, and validating landslide-tsunami numerical models. For instance, Jiang and Leblond [1992, 1993] developed a numerical model to simulate a deformable submarine landslide (mudslide) and the generated surface waves using nonlinear shallow water (SW) equations for both water waves and mudslide material. The numerical model fully coupled the mudslide and the water wave dynamics. Imamura and Imteaz [1995] and Imteaz and Imamura [2001] developed a numerical model for two-layer flows along a variable bottom by using the leap-frog finite difference scheme with a second-order truncation error for the solution of the SW equations. The landslide material was immiscible with uniform density and viscosity and the landslide motion was not prescribed but obtained using internally balanced

forces. Thomson *et al.* [2001] modified a SW numerical model developed by Fine *et al.* [1998] to include arbitrary bottom topography and mudslide viscosity with full two-way interaction. The model was used to simulate the tsunami of 3 November 1994 in Skagway, Alaska. Concurrently, Heinrich *et al.* [2001] developed a SW numerical model to study the efficiency of deep water slumps in producing tsunami waves. The model was tested and validated by comparison with a numerical model that solves the Navier-Stokes (NS) equations. The SW mudslide phase included both, a non-Newtonian friction law and a basal friction coefficient. Through means of a sensitivity test and by applying it to a real tsunami event (PNG), it was concluded that the generated wave depends strongly on the constitutive law of the landslide rheology.

[5] Assier-Rzadkiewicz *et al.* [1997] simulated an underwater landslide using a 2-D fluid mechanics mixture model based on the NS equations. The mudslide material was considered as a viscoplastic fluid with rheological parameters, e.g., the diffusion and viscosity coefficients, the Bingham yield stress and the basal friction. The model was validated with analytical solutions and laboratory experiments documented in Heinrich [1992] for a viscous-Bingham flow and compared against a sliding-rigid box and a gravel slide laboratory experiment. They stressed the importance of the sediment rheology and the diffusion parameter in the wave dynamics. Later, Grilli and Watts [1999, 2005] and Grilli *et al.* [2010], applied fully nonlinear 2-D and 3-D potential flow (Boundary Element Method) simulations of underwater landslide-tsunamis to water wave generation. They assumed geometrically idealized landslide shapes, i.e., for the 2-D, a semiellipse or “bump” configuration and for the 3-D, a bi-Gaussian-shaped or “saucer” configuration. The landslide center of mass motion along the slope was prescribed based on a dynamic force balance using Newton's laws and some empirical coefficients based on theories or validated experimentally. The results obtained in this study were used to create landslide-tsunami sources for practical application of tsunami studies [Tappin *et al.*, 2008].

[6] Another well-known numerical model is the SAGE hydrocode. SAGE has been used in many occasions by modelers to simulate landslide-induced tsunami, Mader and Gittings [2002, 2003] and Gisler [2006]. The code, originally developed by Gittings [1992] for Science Applications International, Los Alamos National Laboratory, is mainly suited in compressible multi-material simulations, e.g., meteorite impact, Gisler *et al.* [2004]. It solves the full set of compressible NS equations, including the equation of state and different constitutive models for material strength. An automatic adaptive Eulerian grid refinement is employed with a high-resolution Godunov scheme. The adaptive mesh can be refined locally where large gradients of certain physical properties of the fluid-flow exist, e.g., pressure, density, etc.

[7] Liu *et al.* [2005] implemented a numerical model to simulate a landslide-generated tsunami. The model solves the 3-D NS equations and is based on the Large Eddy Simulation diffusion mechanism. The Smagorinsky subgrid scale is employed for the turbulence closure. The volume of fluid (VOF) method is used to track the water free surface and the shoreline evolution. To test the model a laboratory experiment was carried out in a large scale wave

tank by using a solid wedge sliding on a plane slope at one end of the tank [Liu *et al.*, 2005; Synolakis *et al.*, 2007].

[8] Kowalik *et al.* [2005a, 2005b] developed a 2-D NS model for waves generation by rigid and deformable moving objects. The standard VOF method was used to track the water free surface and the shoreline evolution. The first order VOF donor-acceptor technique for the fluid advection of Hirt and Nichols [1981] was used by reducing the centered difference approximation (second order) by means of the so-called parameter alpha, i.e., weighting the upstream derivative of the quantity being fluxed more than the downstream derivative. The model's capabilities to simulate a rigid underwater or subaerial landslide for the tsunami generation was achieved by including a dynamic fractional area-volume technique for the transient moving boundaries of the object within the Cartesian grid system. The model results were compared with SW analytical solutions (provided in Synolakis *et al.* [2007]) as well with the solutions obtained by using a SW numerical model. Large differences were observed between the two approaches (2-D NS versus SW) when nonhydrostatic effects were strong, mainly due to the fact that SW model and the SW analytical derivation inherently do not consider the vertical component of velocity/acceleration in their solutions. Later, Horrillo [2006] implemented and tested the model against a subaerial landslide laboratory experiment described in Heinrich [1992]. In this experiment, the 2-D NS model confirmed its capability to deal with complex wave kinematics at early stages of wave generation.

[9] It is noteworthy that even though the SW approximation is relatively accurate in many practical tsunami applications, e.g., cosiesmic-sources in which the resulting waves are usually in the shallow water regime (long waves), it is still doubtful when this approximation is applied to landslide-tsunamis because the landslide motion usually presents large vertical velocity and acceleration which are important for the wave kinematics and free surface evolution. The physical aspect on the wave kinematics is even more critical at early stage of the landslide motion or tsunami generation [Grilli *et al.*, 2002; Fritz *et al.*, 2003a, 2003b; Kowalik *et al.*, 2005a]. In addition, the departing or out-going waves, usually fit in the intermediated depth regime as they reach deeper water from the generation region. Simultaneously, the back-going waves evolve as highly dispersive in the shoaling process toward the coastline.

[10] Abadie *et al.* [2010] reported on the application and experimental validation of a multiple fluid NS model, THE-TIS, for waves generated by idealized slide geometries or deforming slides. The model treated all computational domain regions, i.e., water, air, and slide, as Newtonian fluids. Instead of specifying the slide kinematics, a penalty method was employed to force implicitly the two-way coupling between the rigid slide and the air or water phase. The model has been validated using analytical solutions and several laboratory experiments from previous studies, including the 3-D landslide experiment described in Liu *et al.* [2005] and Synolakis *et al.* [2007].

[11] Application of numerical models to develop practical tsunami hazard/mitigation products, for example tsunami inundation maps, requires model testing over a variety of benchmark problems to ensure model results

match expected values within a minimal margin of errors. In addition, tsunami numerical models need to be continuously tested with new releases or updated versions, or new sets of suited laboratory/tsunami-field data that have become available. Therefore, one of the main objectives of this work is to validate the simplified 3-D NS version derived from the work described in Kowalik *et al.* [2005a, 2005b] and Horrillo [2006]. The simplified 3-D NS tsunami model is specifically customized for tsunami calculations and it is dubbed TSUNAMI3D for Tsunami Solution Using Navier-Stokes Algorithm with Multiple Interfaces. The model was initially developed at the University of Alaska Fairbanks and improved later in Texas A&M University at Galveston. The model is further tested in this study using the laboratory setup described in Liu *et al.* [2005] and Synolakis *et al.* [2007] as 3-D tsunami generation by underwater landslides, see also *National Tsunami Hazard Mitigation Program (NTHMP)* [2012].

[12] It is well known that full 3-D numerical models are highly computationally intensive and require a considerable amount of computer resources. Therefore, the simplified 3-D NS model has been conceived to overcome the computational burden that is common in 3-D tsunami simulations. The simplification is derived from the large aspect ratio (horizontal/vertical scale) of the tsunami wave and the selected computational cell size required to construct an efficient 3-D grid. The large aspect ratio of the tsunami wave requires also a large grid aspect ratio to reduce runtime and memory usage. However, the grid aspect ratio should be smaller than the aspect ratio of the tsunami wave to facilitate the fluid surface reconstruction. The standard VOF algorithm, the donor-acceptor technique of Hirt and Nichols [1981], has been simplified to account for the large aspect ratio of the grid. The pressure term is split in two components, hydrostatic and nonhydrostatic. In addition, this study discusses the effect of using a sharp interface between the mudslide material and the water for a full-scale landslide event in the GOM. In this particular experiment, it is thought that excessive diffusion of certain physical properties (e.g., the averaged-density at a given cell having the water-mudslide interface) originated by the low resolution necessary for efficient numerical computation, might not affect considerably the generated (initial) tsunami wave configuration. To confirm this assertion, a 2-D numerical experiment in x, z (horizontal and vertical) axes is carried out using the simplified 3-D NS model and compared with the commercial Computational Fluid Dynamic (CFD) model FLOW3D. The commercial model uses a diffusive interface between mudslide and water; on the other hand, the simplified 3-D NS model utilizes a sharp (not diffusive) interface condition. Last, a large scale 3-D numerical simulation is carried out for the ancient GOM's East-Breaks landslide by using the simplified model to calculate the early stages of the tsunami wave propagation.

2. Model Description

[13] The simplified 3-D NS numerical model is based on the CFD model development originated in Los Alamos National Laboratory (LANL) during the 1970s following

the work done by C. W. Hirt and a group of researchers, including among others A. A. Amsden, T. D. Butler, L. D. Cloutman, B. J. Daly, R. S. Hotchkiss, C. Mader, R. C. Mjolsness, B. D. Nichols, H. M. Ruppel, M. D. Torrey, and D. B. Kothe. It solves transient fluid flow with free surface boundaries based on the concept of the fractional VOF using an Eulerian mesh of rectangular cells having variable size. The fluid equations solved are the finite difference approximation of the full NS equations and the continuity equation. The basic mode of operation is for a single fluid phase having multiple free surfaces. However, the simplified 3-D NS model also can be used for calculations involving two fluid phases separated by a sharp or diffusive interface, for instance, water and mudslide. In either case, the incompressible fluids are treated as Newtonian. Internal obstacles (topography, wall, etc.) are defined by blocking out fully or partially any desired combination of cells in the domain.

[14] In general, coseismic-generated tsunami waves are very long (>100 km) with wave heights varying from fraction of a meter to several meters. The horizontal-to-vertical (H/V) aspect ratio of a tsunami wave is very large, i.e., wavelength/wave-height of $O(10^4)$. For massive landslide-tsunami, specifically in the region of generation, the initial tsunami wave obtained by numerical simulations is in general shorter and higher if compared with coseismic-generated wave, yet with large H/V aspect ratio, e.g., wavelength/wave-height of $O(10^3)$. The first problem to overcome in a full-scale 3-D tsunami numerical calculation is to identify a computational grid aspect ratio that solves the different scale of the surface interface accurately and efficiently. Computational cell (grid) with aspect ratio smaller than the wavelength/wave-height ratio, e.g., $O(10^2)$ makes surface interface at surface cells to look more horizontal, simplifying the advection algorithm. Simultaneously, the grid aspect ratio should be efficient, large enough not to over resolve the tsunami wave. In this particular study, the standard VOF method of Hirt and Nichols [1981] for tracking the evolution of fluid interfaces has been slightly modified to account for the large H/V aspect ratio of the computational cell that results in the construction of an efficient 3-D structured grid for tsunami calculations. Due to the large horizontal-vertical aspect ratio of a tsunami wave and the smaller horizontal-vertical grid aspect ratio, the fluid interface is assumed to be nearly horizontal in each individual surface cell. The sea level field is calculated based on the VOF function F , by integrating the fluxes of each individual fluid cells column wise (packing method) [Nichols et al., 1980]. The F function accounts for the fractional volume of fluid contained in the cell (water and/or mudslide concentration). A unit value for F corresponds to a fluid cell totally filled with water or mudslide material, while a value of zero indicates an empty cell. Because the fluid is assumed to be nearly horizontal in each individual surface cell, implies that detachment of a parcel of fluid in the vertical direction is not allowed, e.g., breaking waves. The donor-acceptor approach, which prevents overfilling or over-emptying computational fluid cells in the advection process, is simplified by only checking the over-emptying of donor cells (preventing fluxing more fluid than the donor cell has). Overfilling of a computational surface cell is usually advected to the immediate above-

cell in the calculation process of the sea level. The approach although crude by present standard has proved to be valid for cells with an aspect ratio much greater than two ($H/V \gg 2$). Also the assumption completely eliminates the task for the free surface reconstruction. The simplified advection method for tsunami modeling conserves strictly fluid mass in the control volume cell and the total volume error is completely eliminated from the calculations.

[15] The NS equations is solved following the original work of Chorin [1968], the so-called “projection Methods”. In Chorin [1968] method, the NS momentum equation is solved by splitting the equation into two steps. In the first step, an intermediate velocity field is advanced in time using the NS equation without the total pressure gradient term. In the second step, the total pressure and final divergence-free velocity field are determined by solving the linear system of equations resulting from the Poisson’s equation. In the present method, the NS equations is solved in the same manner as the projection method of Chorin [1968], but the total pressure is split into hydrostatic and nonhydrostatic parts [Casulli and Stelling, 1998]. In the first step, the hydrostatic pressure gradient term is retained to advance in time the intermediate velocity field neglecting the nonhydrostatic pressure gradient. The nonhydrostatic pressure gradient field and the final divergence-free velocity are obtained in the same fashion as in the second step of the projection method. The splitting of the pressure term makes possible a hydrostatic solution by merely switching off the second step of the projection method, which reduces the overall solution to a depth integrated approximation. As the hydrostatic pressure gradient term is retained in the first step the advanced in time velocity field can be obtained explicitly. Therefore, the simplified 3-D NS model can be used to discern nonhydrostatic effects from the full solution while maintaining the three dimensional structure. The model is suitable for complex tsunami generation mechanisms because it has built-in capabilities for: (a) moving or deformable objects; (b) subaerial/subsea landslide sources; (c) simplified soil rheology, and (d) complex vertical or lateral bottom deformation.

[16] The model is in constant development and requires a high performance FORTRAN compiler. Usually a 3-D simulation requires a large amount of computer memory and CPU-wall-time to obtain the solution. The most computational demanding subroutines are parallelized using MPI and OPENMP directives.

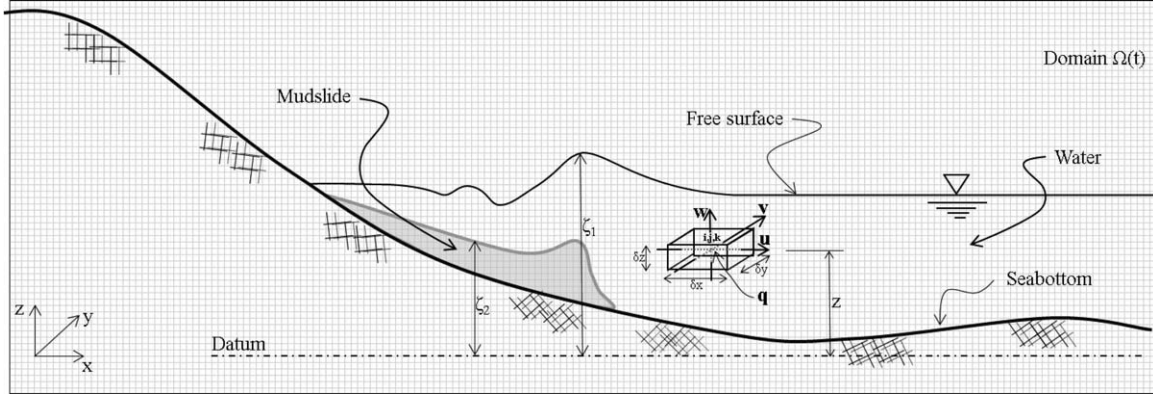
3. Model Governing Equations

[17] The governing equations to describe the flow of two incompressible Newtonian fluids (e.g., water and mudslide, see Figure 1) on domain $\Omega(t)$ are the incompressibility condition equation,

$$\frac{\partial u}{\partial x} + \frac{\partial v}{\partial y} + \frac{\partial w}{\partial z} = 0 \quad (1)$$

which results from the continuity equation when the density is constant, and the nonconservative equation of momentum given by

1. For the water phase


Figure 1. Model domain sketch.

$$\begin{aligned} \frac{\partial u}{\partial t} + u \frac{\partial u}{\partial x} + v \frac{\partial u}{\partial y} + w \frac{\partial u}{\partial z} = -g \frac{\partial \eta_1}{\partial x} - \frac{1}{\rho_1} \frac{\partial q}{\partial x} + \frac{\partial}{\partial x} \left[\frac{\mu_1}{\rho_1} \left(2 \frac{\partial u}{\partial x} \right) \right] \\ + \frac{\partial}{\partial y} \left[\frac{\mu_1}{\rho_1} \left(\frac{\partial u}{\partial y} + \frac{\partial v}{\partial x} \right) \right] + \frac{\partial}{\partial z} \left[\frac{\mu_1}{\rho_1} \left(\frac{\partial u}{\partial z} + \frac{\partial w}{\partial x} \right) \right] \end{aligned} \quad (2)$$

$$\begin{aligned} \frac{\partial v}{\partial t} + u \frac{\partial v}{\partial x} + v \frac{\partial v}{\partial y} + w \frac{\partial v}{\partial z} = -g \frac{\partial \eta_1}{\partial y} - \frac{1}{\rho_1} \frac{\partial q}{\partial y} + \frac{\partial}{\partial x} \left[\frac{\mu_1}{\rho_1} \left(\frac{\partial v}{\partial x} + \frac{\partial u}{\partial y} \right) \right] \\ + \frac{\partial}{\partial y} \left[\frac{\mu_1}{\rho_1} \left(2 \frac{\partial v}{\partial y} \right) \right] + \frac{\partial}{\partial z} \left[\frac{\mu_1}{\rho_1} \left(\frac{\partial v}{\partial z} + \frac{\partial w}{\partial y} \right) \right] \end{aligned} \quad (3)$$

$$\begin{aligned} \frac{\partial w}{\partial t} + u \frac{\partial w}{\partial x} + v \frac{\partial w}{\partial y} + w \frac{\partial w}{\partial z} = -\frac{1}{\rho_1} \frac{\partial q}{\partial z} + \frac{\partial}{\partial x} \left[\frac{\mu_1}{\rho_1} \left(\frac{\partial w}{\partial x} + \frac{\partial u}{\partial z} \right) \right] \\ + \frac{\partial}{\partial y} \left[\frac{\mu_1}{\rho_1} \left(\frac{\partial w}{\partial y} + \frac{\partial v}{\partial z} \right) \right] + \frac{\partial}{\partial z} \left[\frac{\mu_1}{\rho_1} \left(2 \frac{\partial w}{\partial z} \right) \right] \end{aligned} \quad (4)$$

where $u(x, y, z, t)$, $v(x, y, z, t)$, and $w(x, y, z, t)$ are the velocity components along the coordinate axes of the fluid at point $\mathbf{x} = x\hat{i} + y\hat{j} + z\hat{k}$ and time t . Here, subscript 1 indicates physical parameters or variables corresponding to the water phase, i.e., $\eta_1(x, y, t)$ is the water-surface elevation measured from the vertical datum, ρ_1 is the density of the water, and g is the acceleration due to gravity. Considering the water phase as a Newtonian fluid, the kinematic viscosity μ_1/ρ_1 can be adjusted to give the best possible agreement with the reference data. The total pressure, $p = p_{hyd} + q$, has been divided into a hydrostatic pressure

$$p_{hyd} = \rho_1 g (\eta_1 - z) \quad (5)$$

and the nonhydrostatic pressure q such that $\partial p_{hyd} / \partial z = -\rho_1 g$. Here, z is the elevation measured from the vertical datum to the cell center.

2. For the mudslide phase

$$\begin{aligned} \frac{\partial u}{\partial t} + u \frac{\partial u}{\partial x} + v \frac{\partial u}{\partial y} + w \frac{\partial u}{\partial z} = -g \left(\alpha \frac{\partial \eta_1}{\partial x} + (1 - \alpha) \frac{\partial \eta_2}{\partial x} \right) \\ - \frac{1}{\rho_2} \frac{\partial q}{\partial x} + \frac{\partial}{\partial x} \left[\frac{\mu_2}{\rho_2} \left(2 \frac{\partial u}{\partial x} \right) \right] + \frac{\partial}{\partial y} \left[\frac{\mu_2}{\rho_2} \left(\frac{\partial u}{\partial y} + \frac{\partial v}{\partial x} \right) \right] \\ + \frac{\partial}{\partial z} \left[\frac{\mu_2}{\rho_2} \left(\frac{\partial u}{\partial z} + \frac{\partial w}{\partial x} \right) \right] \end{aligned} \quad (6)$$

$$\begin{aligned} \frac{\partial v}{\partial t} + u \frac{\partial v}{\partial x} + v \frac{\partial v}{\partial y} + w \frac{\partial v}{\partial z} = -g \left(\alpha \frac{\partial \eta_1}{\partial y} + (1 - \alpha) \frac{\partial \eta_2}{\partial y} \right) - \frac{1}{\rho_2} \frac{\partial q}{\partial y} \\ + \frac{\partial}{\partial x} \left[\frac{\mu_2}{\rho_2} \left(\frac{\partial v}{\partial x} + \frac{\partial u}{\partial y} \right) \right] + \frac{\partial}{\partial y} \left[\frac{\mu_2}{\rho_2} \left(2 \frac{\partial v}{\partial y} \right) \right] + \frac{\partial}{\partial z} \left[\frac{\mu_2}{\rho_2} \left(\frac{\partial v}{\partial z} + \frac{\partial w}{\partial y} \right) \right] \end{aligned} \quad (7)$$

$$\begin{aligned} \frac{\partial w}{\partial t} + u \frac{\partial w}{\partial x} + v \frac{\partial w}{\partial y} + w \frac{\partial w}{\partial z} = -\frac{1}{\rho_2} \frac{\partial q}{\partial z} + \frac{\partial}{\partial x} \left[\frac{\mu_2}{\rho_2} \left(\frac{\partial w}{\partial x} + \frac{\partial u}{\partial z} \right) \right] \\ + \frac{\partial}{\partial y} \left[\frac{\mu_2}{\rho_2} \left(\frac{\partial w}{\partial y} + \frac{\partial v}{\partial z} \right) \right] + \frac{\partial}{\partial z} \left[\frac{\mu_2}{\rho_2} \left(2 \frac{\partial w}{\partial z} \right) \right] \end{aligned} \quad (8)$$

where subscript 2 represents physical parameters and variables corresponding to the mudslide phase. $\eta_2(x, y, t)$ is the mudslide-surface elevation measured from the vertical datum, ρ_2 is the mudslide material density, and α is the water-mudslide density ratio given by ρ_1/ρ_2 . The total pressure $p = p_{hyd} + q$ has been divided into the hydrostatic pressure

$$p_{hyd} = g [\rho_1 (\eta_1 - \eta_2) + \rho_2 (\eta_2 - z)] \quad (9)$$

and the dynamic pressure q . The mudslide material is considered as a Newtonian fluid, however, the kinematic viscosity, μ_2/ρ_2 and friction term, can be adjusted according to a constitutive model for mudslide rheology, e.g., Bingham model, which is not covered or used in this study.

[18] Subsea soil material in the GOM might be fluidized by external triggered mechanisms, e.g., high sediment rate, earthquake, shallow stratigraphic layers with overpressured pore water, salt intrusion movement, oversteepening of shelf edge, and possibly gas hydrates or combination of these mechanisms. At early state of the mudslide downslope movement, a Newtonian fluid approach for the mudslide material could be valid if one seeks for a conservative estimation of the initial tsunami wave. It is also true that a Newtonian fluid will not come to rest completely. However, this last stage of the mudslide evolution occurs in deeper water or in the ocean basin with minor consequence to the tsunami characteristics. Massive landslides have longer runout distances; basal-friction and shear-rate seem to reduce as the mudslide thickness/volume increases, the larger the slide volume, the greater the thickness and the smaller the shear rate [Campbell *et al.*, 1995]. Therefore, assuming no basal friction at the initial state of the wave

generation or even assuming inviscid flow for the Mudslide-water phases is a valid and conservative supposition. The geological footprint in deeper water of large fan systems in the GOM generated by ancient submarine landslides supports this simplified assumption of a Newtonian fluid for the mudslide material.

[19] For the discretization of the computational domain, the model uses an Eulerian variable mesh of rectangular cells with large aspect ratio. The governing equations are solved by using the standard finite difference scheme starting with field variables such as \mathbf{u} , q , and η are known at time $t = 0$. The sealevel or mudslide interface location η is a function of F (obtained by the VOF method) and is known once F is determined. All variables are treated explicitly with the exception of the nonhydrostatic pressure field q , which is implicitly determined. The governing equations are solved by discretizing the field variables spatially and temporally in the domain to obtain new field variables at any required time. Nonlinear terms are approximated by using an upstream/downstream approach up to the third order. The hydrodynamic pressure field q is calculated through the Poisson's equation by using the incomplete Choleski conjugated gradient method to solve the resulting linear system of equations.

[20] The velocities u , v , and w associated with a computational cell is located at the right, back, and the top cell faces as indicated in Figure 1. The nonhydrostatic $q(x, y, z, t)$ and the hydrostatic pressures are located at the cell center.

[21] To solve numerically the nonlinear terms, the third-order backward finite difference for a variable grid size system is used. For example, in the x direction and positive fluid velocity at the cell face ($u_{i,j,k} > 0$), the third-order finite difference form reads

$$\begin{aligned} u \frac{\partial u}{\partial x} \approx & u_{i,j,k} \left[\left(\frac{\delta x_i (\delta x_{i-1} + \delta x_i)}{\delta x_{i+1} (\delta x_i + \delta x_{i+1}) (\delta x_{i-1} + \delta x_i + \delta x_{i+1})} \right) u_{i+1,j,k} \right. \\ & + \left(\frac{(\delta x_{i+1} - \delta x_i) (\delta x_{i-1} + \delta x_i) + \delta x_i \delta x_{i+1}}{\delta x_i \delta x_{i+1} (\delta x_{i-1} + \delta x_i)} \right) u_{i,j,k} \\ & - \left(\frac{\delta x_{i+1} (\delta x_{i-1} + \delta x_i)}{\delta x_{i-1} \delta x_i (\delta x_i + \delta x_{i+1})} \right) u_{i-1,j,k} \\ & \left. + \left(\frac{\delta x_i \delta x_{i+1}}{\delta x_{i-1} (\delta x_{i-1} + \delta x_i) (\delta x_{i-1} + \delta x_i + \delta x_{i+1})} \right) u_{i-2,j,k} \right] \end{aligned} \quad (10)$$

[22] When the grid size is uniform or constant, equation (10) reduces to

$$u \frac{\partial u}{\partial x} \approx \frac{u_{i,j,k}}{6\delta x} [2u_{i+1,j,k} + 3u_{i,j,k} - 6u_{i-1,j,k} + u_{i-2,j,k}] \quad (11)$$

[23] The nonlinear term approximation is built assuming a gradual variations in cell sizes to minimize the reduction in approximation order. In regions where maximum resolution is desired, cell sizes are initially equal to the minimum value specified and slowly expanded quadratically as cells depart from the region of interest. If the gradual variation in cell sizes is done adequately, the order of the approximation should be close to third order [Hirt and Nichols, 1981]. The third-order finite difference form of the advective terms for variable grid size can be found in more detail in Horrillo [2006].

[24] Both interfaces, water and mudslide surface elevations, are traced using a simplified VOF method based on the donor-acceptor algorithm of Hirt and Nichols [1981]. The simplified VOF method defined by the scalar function $F_{1,2}(x, y, z, t)$ determines the water and the mudslide regions in space and time. Where F_1 is the fraction function for the water in the computational cell, whereas F_2 is fraction function for the mudslide. A unit value for F_1 or F_2 corresponds to a fluid cell totally filled with water or mudslide material, respectively; while a value of zero indicates an empty cell. Therefore, a fluid cell with value between 0 and 1 for F_1 and having an immediate neighbor empty cell indicates a surface cell. In the same manner, a fluid cell with value between 0 and 1 for F_2 and having an empty or a neighbor water-flooded cell indicates a mudslide-air or mudslide-water interface cell, respectively. The equation describing both scalar functions, F_1 and F_2 , is given by

$$\frac{dF_{1,2}}{dt} = \frac{\partial F_{1,2}}{\partial t} + \frac{\partial u F_{1,2}}{\partial x} + \frac{\partial v F_{1,2}}{\partial y} + \frac{\partial w F_{1,2}}{\partial z} = 0 \quad (12)$$

which states that $F_{1,2}$ propagates with the fluid velocity $\mathbf{u} = u\hat{i} + v\hat{j} + w\hat{k}$. Physical properties in each cell element, i.e., the density and viscosity, can be weighted in terms of the $F_{1,2}(x, y, z, t)$ function. For example, a general expression for the cell density is determined by the following equation and conditions,

$$\begin{aligned} \rho(x, y, z, t) &= \rho_1(F_1 - F_2) + \rho_2 F_2 \\ F_1 &= 1.0, \text{ for cells below water level.} \\ F_1 &= F_2, \text{ for cells above water level.} \end{aligned} \quad (13)$$

[25] Equation (13) can be explained with the help of the following examples: If the control volume cell happens to be below the water level (completely submerged) and inside the mudslide material, i.e., $F_1 = 1.0$ and $F_2 = 1.0$; then, the density $\rho(x, y, z, t) = \rho_2$. If the cell happens to be below the sealevel but has the mudslide-water interface, e.g., with 30% of mudslide material, i.e., $F_1 = 1.0$ and $F_2 = 0.30$; then, the density $\rho(x, y, z, t) = 0.7\rho_1 + 0.3\rho_2$. Now, in case a cell happens to be above the water level (subaerial landslide), then F_1 equals F_2 , whatever the condition the cell is in, e.g., completely submerged into the mudslide ($F_1 = F_2 = 1.0$) or having a mudslide-air interface ($0 < F_1 = F_2 < 1$); then, the density is $\rho(x, y, z, t) = \rho_2 \times F_2$. The interpretation of equation (13) and conditions, suggests that advection of mudslide material above the water level requires the existence of water as a medium of transportation. This artifact greatly simplifies the calculations of both free surfaces, since the advection algorithm for the mudslide material is an external procedure that is completed once the advection of water is done.

[26] Both scalar function F_1 and F_2 are located at the cell center as the nonhydrostatic pressure q . Equation (12) is solved in the water and mudslide fluid phases, and all empty cells located immediately next to the fluid phases. The water and mudslide surface elevations $\eta_{1,2}(x, y, t)$ are a mere byproduct of $F_{1,2}$ and they are calculated by integrating $F_{1,2}$ along the fluid column at each x, y location at time t . This implies that multiple values for the surface or separation of the fluid in the vertical direction are not allowed, since there is only one value for η_1 and η_2 at each x, y location. This

assertion is valid for cells with aspect ratio much greater than two ($H/V \gg 2$), which is commonly used in mesh generation of numerical models for full-scale tsunamis.

[27] One of the major constraints in 3-D tsunami numerical simulation is the limitation imposed by the computing time or memory requirement to solve the several physical scales of a landslide-tsunami, i.e., water and mudslide free surfaces, runup, etc. The construction of an efficient computational grid becomes one of the most important aspect in the process to obtain accurate results. Usually, in the process, the modeler should achieve an efficient grid size, until increasing the grid resolution has marginal effects on results and further refining would become unnecessary. This is not always the case for the majority of the 3-D large-scale numerical simulations, where the chosen grid resolution is a compromise between accuracy and computer performance.

[28] Another equally important aspect is that numerical models intrinsically have their own numerical diffusion or friction, which arises mainly from the chosen discrete approximation of the momentum advection, which is further affected by the space and time steps selected. This is greatly exacerbated when the grid resolution obtained by the compromise between accuracy and performance is coarse. Therefore, for the sake of simplicity and numerical efficiency, a turbulence closure method is not considered in the model solution, instead, the scale of turbulence is mainly accomplished using the general viscous coefficient described by the two phase fluids, water and mudslide, usually obtained by a trial and error adjustment. This implies that the Direct Numerical Simulation (DNS) approximation is inherent in the numerical model structure; however, this DNS is correctly applied in case the computational domain is relatively well resolved spatially and timely. In many situations, e.g., tsunami generation by landslide on a steep slope, the energy transfer mechanisms is mainly the pressure. In this case, the transient energy loss due to turbulence is expected to be small and comparable to other numerical and physical process losses. Even though the turbulence mechanism is not solved completely in this study, the overall solution is expected to be adequate in the majority of full-scale landslide-tsunami cases.

[29] The friction term in the momentum equation can be adjusted to mimic the internal friction within the fluid body, i.e., the viscosity coefficient. This coefficient has been chosen to give the best possible agreement with the reference data. For instance, in practical application of numerical modeling to reproduce a laboratory experiment using the simplified 3-D NS model, a value for the water viscosity coefficient, μ_1/ρ_1 , typically ranges between 10^{-6} m²/s and 10^{-5} m²/s. On the other hand, for the deformable mudslide, a typical value for μ_2/ρ_2 ranges between 10^{-3} m²/s and 10^1 m²/s [Abadie et al., 2010, 2008]. At the water-mudslide interface a similar expression as indicated for density in equation (13) applies to weight the viscosity according to the water-mudslide concentration. Thus, the viscosity expression for the water-mudslide interface cells reads

$$\frac{\mu}{\rho}(x, y, z, t) = \frac{\mu_1}{\rho_1}(F_1 - F_2) + \frac{\mu_2}{\rho_2}F_2. \quad (14)$$

[30] For a well-resolved domain (finer spatial resolution), additional friction mechanisms often are considered

in the model, for instance, the no-slip condition. The no-slip condition enforces a linear decay of the velocity at all computational cells in contact with the sea-bottom or walls, i.e., $\partial \mathbf{u} / \partial z \neq 0$. Another mechanism that is often implemented to mimic further the bottom friction or the drag-flow resistance in presence of vegetation and debris is by means of linear function which increases the fluid viscosity coefficient to one or several orders of magnitude at computational fluid cells located at a short distance from the sea-bottom or walls [Gelfenbaum and Smith, 1986]. However, this mechanism is topic of a parallel and long-term effort and it is not covered or used in this present work.

4. Laboratory Experiments

[31] It is considered important for any tsunami numerical model to be evaluated against standard benchmarking cases suggested by the NTHMP's standard [OAR PMEL 135, Synolakis et al., 2007]. These benchmarking cases were to be developed to ensure sufficient reliability in the development of tsunami inundation maps, as well as a basic level of consistency between parallel numerical modeling efforts. Herein the 3-D landslide experiment case has been chosen from the standard OAR PMEL 135 to validate the simplified 3-D NS model for tsunami generation caused by underwater landslides. This 3-D laboratory experiment was carried out at Oregon State University by Liu et al. [2005]. In the 3-D laboratory experiments, a solid wedge was used in a large wave tank to represent an underwater landslide-induced tsunami waves, see Figure 2. The solid wedge has a triangular section with a horizontal length of 0.91 m, height of 0.455 m, and width of 0.61 m. The wedge rests in the sloping bottom of the wave tank and it is released from repose. To generate waves with different levels of energy and characteristics, the horizontal surface of the wedge was positioned at different small distances Δ from the still water level. Detailed information of this experiment and link to the reference data are found in *Tsunami Generation and Runup Due to 3-D Landslide* [Synolakis et al., 2007]. The simplified 3-D NS model was tested against the experimental data for cases $\Delta=0.025$ m and $\Delta=0.10$ m. Figure 3 shows a set of snapshots obtained from the simplified 3-D NS model's results for case $\Delta=0.025$ m. Domain dimension, free surface elevation and velocity vectors projected at plane $y=0$ for time $t=1.0, 1.5, 2.0, 2.5$ s are displayed. For numerical efficiency, the domain has been reduced in half by cutting it through its plane of symmetry at $y=0$. The dimension of the computational box in the x, y , and z directions is 6.10 m, 1.85 m, and 3.05 m, respectively. The optimum total number of computational cells is ~ 4.6 millions ($246 \times 76 \times 246$). Consequently, space step or cell size is $0.025 \text{ m} \times 0.025 \text{ m} \times 0.0125 \text{ m}$ in the x, y , and z direction, respectively. This grid was selected by doing a sensitivity test (trying several grid sizes) which is summarized in Figure 4. The selected grid size is a compromise between accuracy and the limitations imposed by computer performance. The grid size is slightly finer than the reported by Liu et al. [2005] of $0.0391 \text{ m} \times 0.074 \text{ m} \times 0.0196 \text{ m}$. Inspection of Figure 4 shows that the mean-normalized error (ERR) of the wave time series (defined later) varied more nearly with the horizontal spacing δx , at least for the coarse grids, yielding an accuracy of $O(\delta x^1)$; for example,

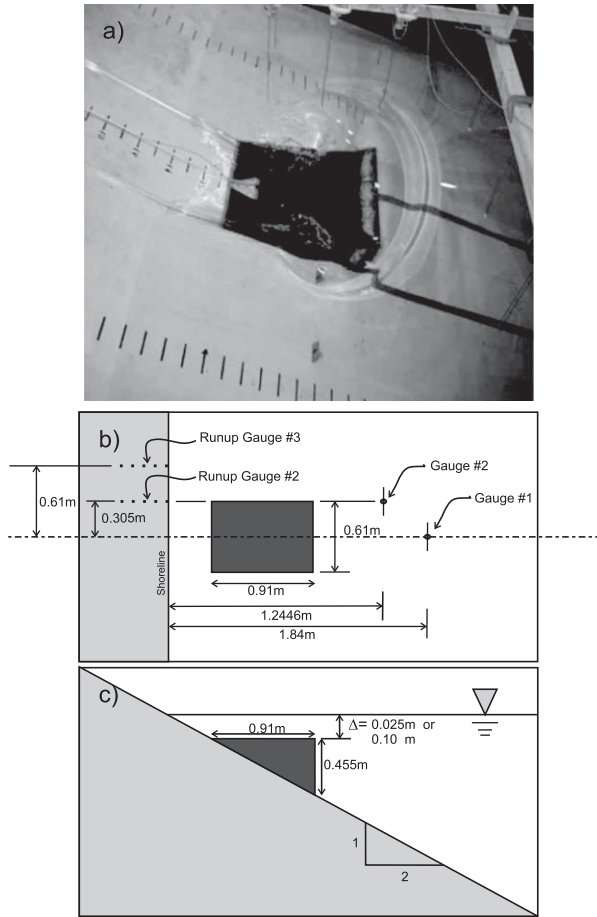


Figure 2. (a) Laboratory experiment snapshot at the moment the solid wedge is going down slope generating a train of waves, *Liu et al.* [2005]. (b and c) Plan and side view schematics of the laboratory experiment setup as described in *Synolakis et al.* [2007] for benchmark problem: *Tsunami Generation and Runup Due to 3-D Landslide*.

if δx is halved, the mean-normalized error is halved too. A grid convergence was immediately achieved on the third try as can be gleaned in Figure 4 from the set of grid size tests.

[32] In tsunami full-scale calculation, the required grid resolution is usually determined by the expected tsunami wavelength. For numerical simulation involving long waves, a horizontal resolution of 20 cells or discretization points per wavelength is recommended as minimum [*Titov and Synolakis, 1997; Shuto, 1991*]. For cases where dispersive waves are expected to develop on the top of the main tsunami wave, e.g., fission of the main tsunami wave into smaller ones or a wave front followed by a train of secondary waves, then the grid resolution should be increased accordingly to the dispersive wavelength required to be solved. Similarly, to simulate numerically *Liu et al.* [2005]’s experiment (a small scale case) was necessary to use a resolution of 40 cells per wavelength (horizontal direction) as minimum; and 5 cells per wave-height (vertical direction) for the expected shoreline oscillation or runup.

[33] Once the computational grid has been defined, several conditions or inequalities for numerical stability are considered for the time step (δt) to guaranty that it is below to certain critical values. For example: first, a parcel of fluid cannot travel more than one cell width per time step. The advection of the F function, as well as the momentum advection, is approximated explicitly in time. Typically, δt is chosen to be some fraction of a minimum value by using the Courant-Friedrichs-Lewy (CFL) condition, which is controlled by the factor N_{CFL} . This condition must be enforced along all coordinate directions, so the transport time step δt , is taken as the minimum of the transport time step of the x direction, y direction, and z direction, thus

$$\delta t < N_{CFL} \times \min \left(\frac{\delta x_i}{|u_{i,j,k}|}, \frac{\delta y_j}{|v_{i,j,k}|}, \frac{\delta z_k}{|w_{i,j,k}|} \right) \quad (15)$$

[34] The factor N_{CFL} should be less than 1.0 in theory, or more conservatively, less than 1/2 in practice. Although a N_{CFL} value closer to 1 is often sought to obtain better accuracy and improve computer performance, a value of $N_{CFL} = 1/3$ was used in this experiment, allowing at least three time steps for the transit of any parcel of fluid throughout the cell. Second, the frictional or diffusion term is evaluated using old time velocity field. This explicit treatment is therefore subjected to a linear stability time step constraint which is evaluated conservatively considering the spatial steps, thus

$$\delta t < \frac{\rho}{2\mu} \left(\frac{1}{\delta x_i^2} + \frac{1}{\delta y_j^2} + \frac{1}{\delta z_k^2} \right)^{-1} \quad (16)$$

[35] If an explicit method is used, the diffusive effect is confined to the neighboring grid cells which leads to the stability bound in equation (16) that limits the time step to be proportional to the square of spatial steps. When the diffusion coefficient is very small, then the N_{CFL} requirement for advection may dominate the numerical stability but as the grid is refined or the diffusion coefficient is large, then the diffusion limit could come into play.

[36] Both stability conditions are only approximate, since they are based on the linear von Neumann analysis, which does not include the simultaneous effect of the pressure gradient in the momentum equation. Finally, with δt chosen to satisfy above inequalities (equations (15) and (16)), then the advection flux is reevaluated. If the advection flux $u\delta t A_f$ exceeds the permissible flux volume $N_{CFL} dx A_f$ (evaluation in the x direction, where A_f is the flux boundary area perpendicular to the x direction flow), i.e., $u\delta t > N_{CFL} dx$, the time step δt is reduced by an adaptive time stepping algorithm and all calculations are restarted with the reduced δt .

[37] To simulate numerically *Liu et al.* [2005]’s experiment, the adaptive time stepping δt is mostly governed by the CFL condition with maximum value permissible of 0.001 s as the model has been adjusted for internal friction with a small value of 10^{-6} m²/s. The no-slip condition is used for the sea-bottom friction. The solid wedge motion was prescribed into the simplified 3-D NS model according to the wedge location time series indicated in *Synolakis et al.* [2007]. The computation time to reproduce 4 s of the physical experiment took 5 h using a PC with 8 CPUs.

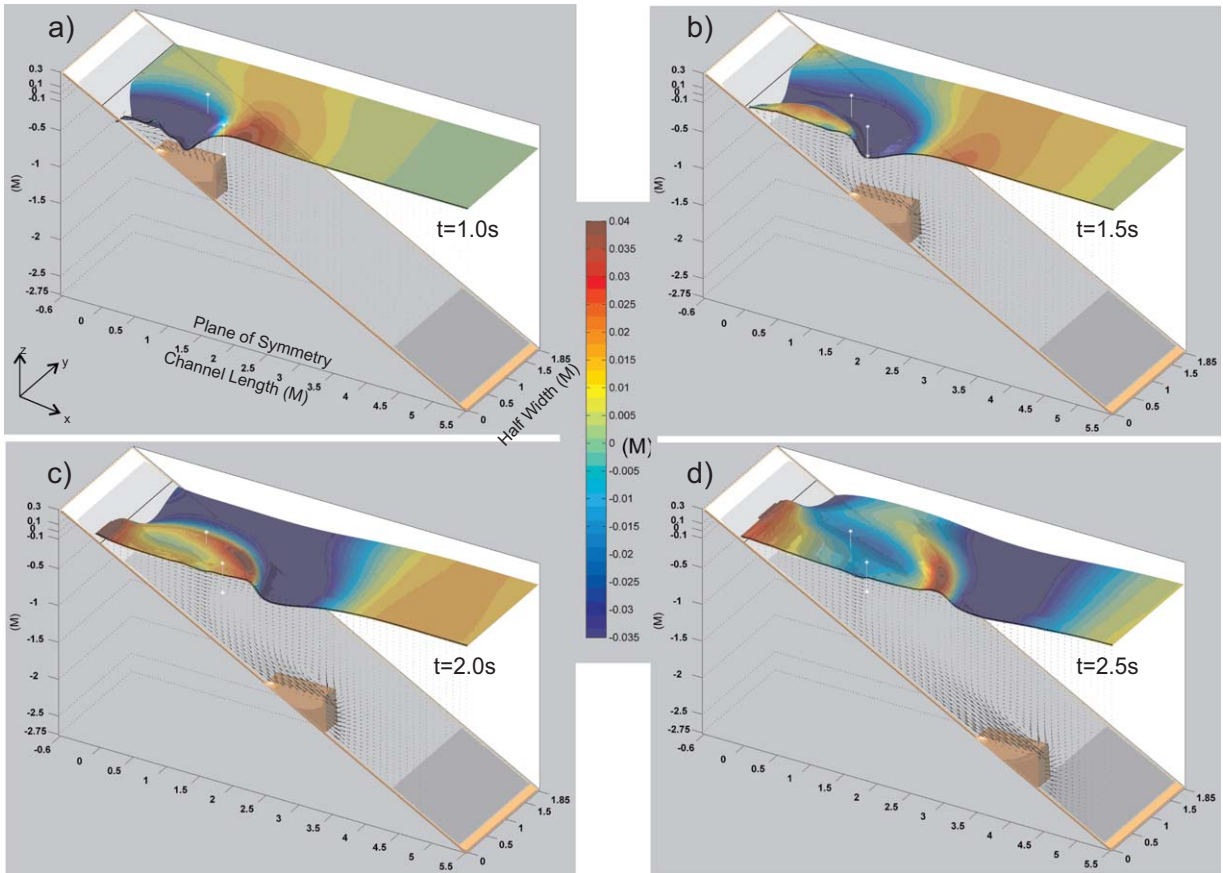


Figure 3. Numerical results sequence of the solid wedge-induced waves for case $\Delta=0.025$. Snapshots are taken from the simplified 3-D NS model results at time $t=[1.0, 1.5, 2.0$ and $2.5]$ s, respectively.

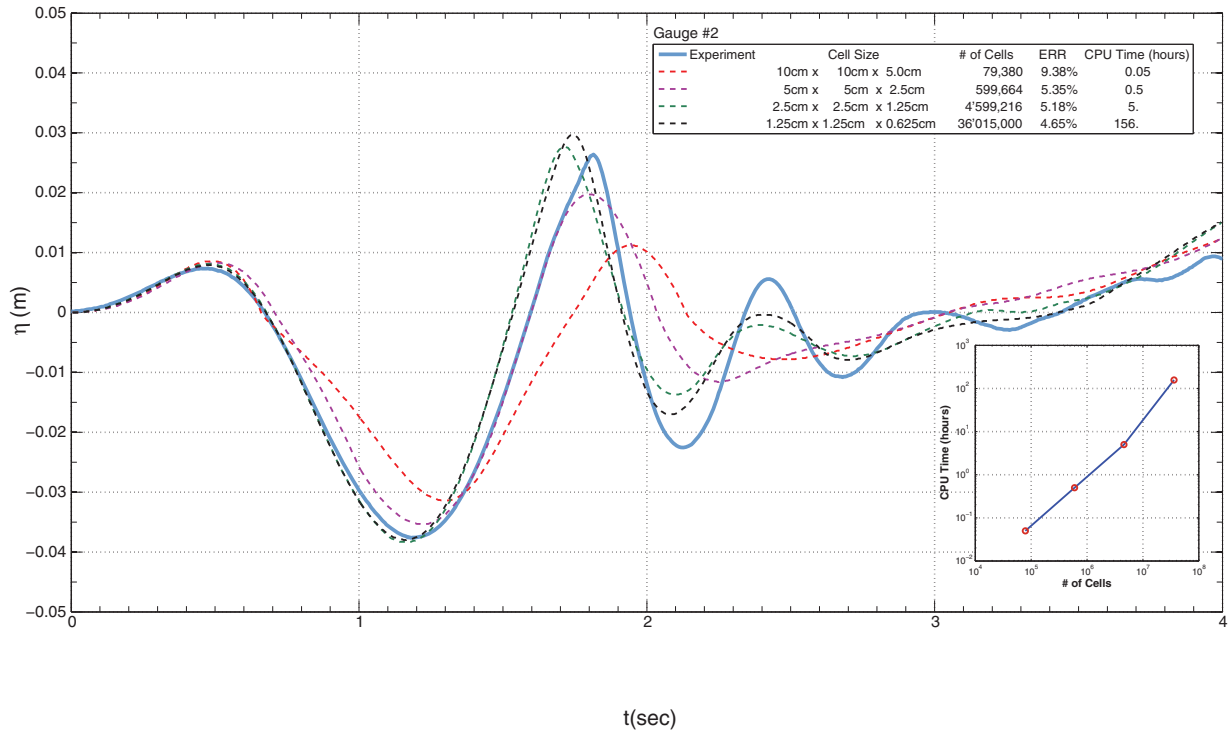


Figure 4. Grid sensitivity test using case $\Delta=0.10$ m at Gauge #2. Grid sensitivity test shows that the optimum (accuracy-performance) grid size is 0.025 m \times 0.025 m \times 0.0125 m.

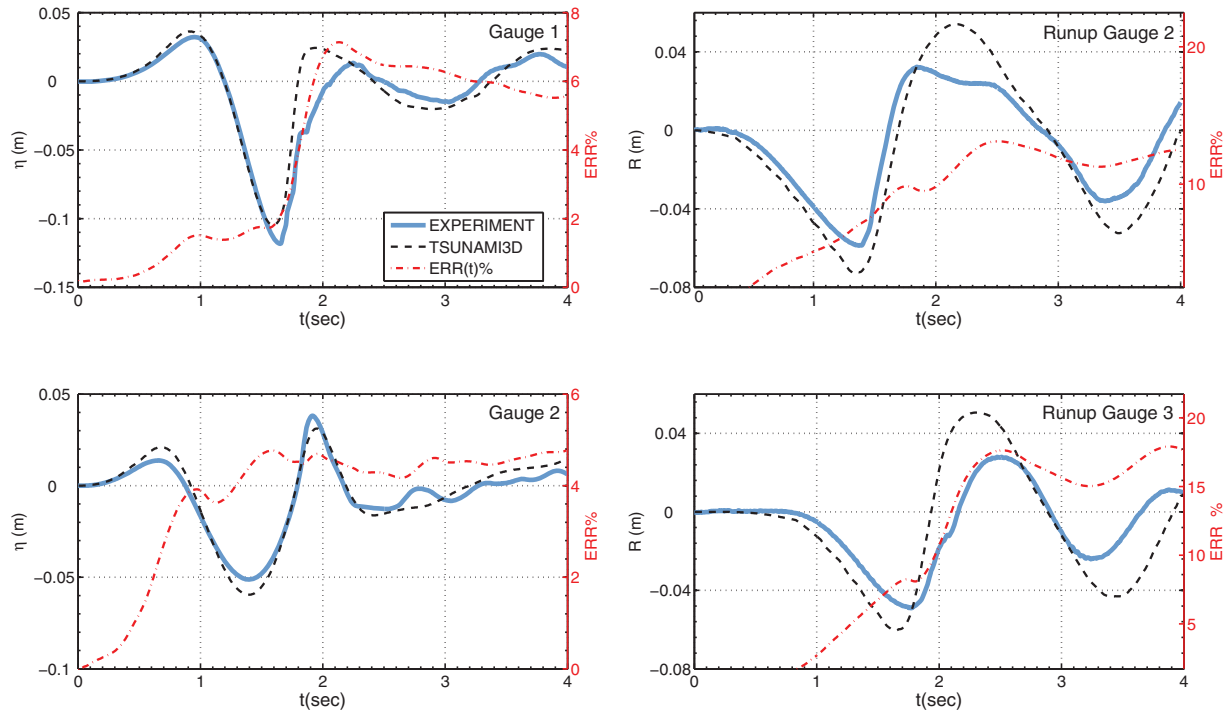


Figure 5. Comparison of the simplified 3-D NS model result (broken-black line) against experiment (solid line) for case $\Delta=0.025$ m. Red line indicates the mean-normalized error up to time t .

[38] The simplified 3-D NS model's results are portrayed against the experiment reference data in Figures 5 and 6. Overall numerical results of the free surface profile agree fairly well with experiment results. Some discrepancies in timing are evident especially in the runup results. The rebound wave for case $\Delta=0.025$ m, specifically the second wave recorded by Gauge #1 which results from the drag of the wedge, is slightly overestimated by the model. The small discrepancy is mainly attributed to numerical friction and to the transient energy dissipation by turbulence processes at early state of the slide initiation. As it was mentioned before, turbulence dissipation mechanism is not considered in the model, assuming that energy loss due to this effect is transient and small.

[39] The mean-normalized error (ERR) shown in Figures 5 and 6 (red line) is used to measure model accuracy up to certain time. The ERR is defined as

$$\text{ERR}(t) = \frac{1}{\zeta_{e_{\max}} - \zeta_{e_{\min}}} \frac{\sum_{i=1}^{n(t)} |\zeta_{e,i} - \zeta_{m,i}|}{n(t)} \quad (17)$$

where $\text{ERR}(t)$ is the mean-normalized error up to time t between the sea level values predicted by the model (ζ_m) and the values observed in the physical experiment (ζ_e). The error is normalized with respect to the difference between the maximum and minimum sea level values obtained in the laboratory experiment ($\zeta_{e_{\max}} - \zeta_{e_{\min}}$), which usually corresponds to the first or second wave height. $n(t)$ is the number of recorded sea levels at a given point (Gauges) up to time t ; therefore, model's errors are function of time. The mean-normalized error up to time t per-

mits visualization of the model's accuracy for the first, second, and subsequent waves. For instance, case $\Delta=0.025$ m in Gauge 1 (Figure 5), the mean-normalized errors up to time $t=[0.95, 2.25, 3.80]$ s are $\text{ERR}(t)=[1.7\%, 6.8\%, 5.6\%]$, respectively. Note that selected times correspond to the occurrence of the first, second, and third maximum wave amplitudes.

5. Full-Scale Tsunami Experiments

[40] Modeling a full-scale 3-D submarine landslide and the waves it generates on a large domain requires a relatively low spatial resolution to circumvent computer overload. Nevertheless, the limited resolution should be adequate enough to obtain a reasonable convergence and time-efficient solution. Physical properties in regions of large gradients tend to diffuse faster when low spatial resolution is used, e.g., the density. Thus, it is alleged that keeping a sharp interface between the mudslide and the water phase would minimize the excessive diffusion problem originated by the low resolution necessary for efficient numerical computation. In addition, the excessive diffusion problem might affect the initial tsunami wave kinematics due to the net energy transfer from the moving slide mass to the water is reduced. To investigate these two interface conditions (sharp and diffusive), a 2-D numerical case study with x, z (horizontal and vertical) axes is carried out using the simplified 3-D NS model and compared with a commercial CFD program, FLOW3D. The 3-D numerical models adopt a channel domain configuration with lateral confinement to represent the 2-D numerical experiment. This is achieved by using few computational cells along

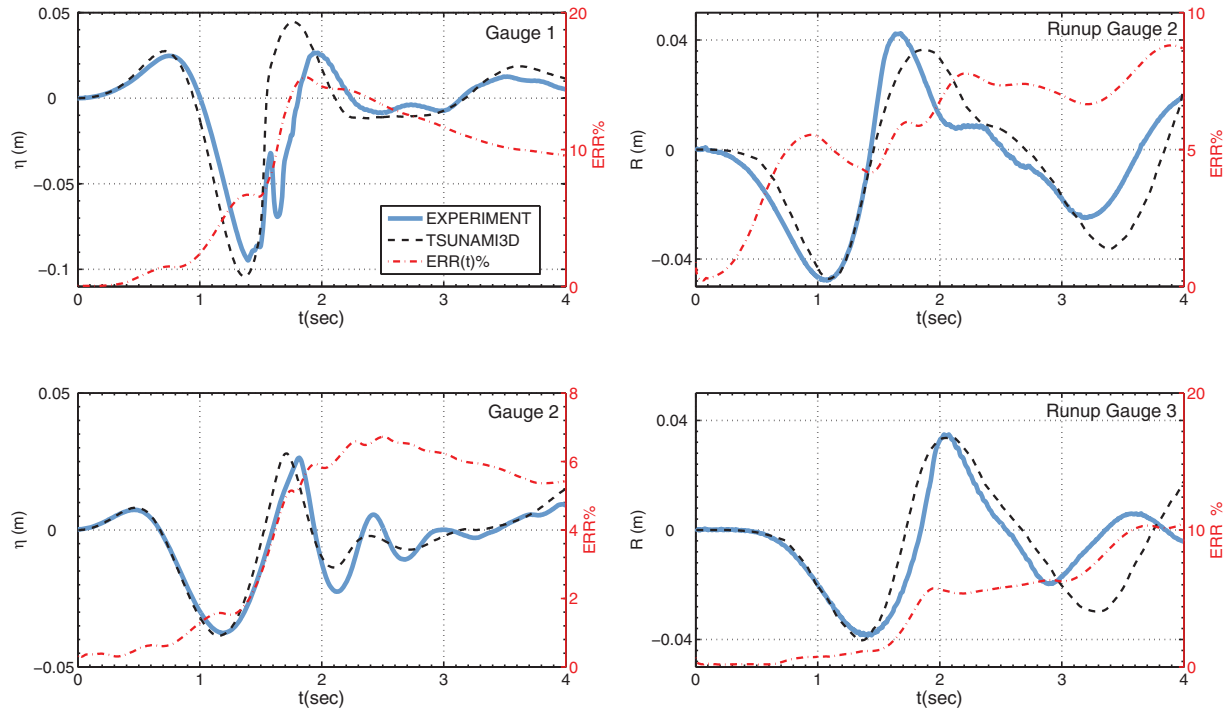


Figure 6. Comparison of the simplified 3-D NS model result (broken-black line) against laboratory experiment (solid line) for case $\Delta=0.10$ m. Red line indicates the mean-normalized error up to time t .

the channel width or y direction and by providing lateral walls along the channel length with full reflecting boundary conditions. The commercial CFD program uses a diffusive interface between mudslide and the water, whereas the simplified 3-D NS model uses a sharp interface condition. Besides, the numerical experiment serves also to compare and validate both models for full-scale landslide-tsunami scenarios.

[41] The 2-D numerical experiment is based on the East-Breaks landslide scenario. The East-Breaks landslide, which lies offshore of the Rio Grande River system is specifically located in the salt province in the north-western part of the GOM. This landslide occurred during the last lowstand of sea level and was the result of the failure of the shelf edge delta, which had accumulated sediment from the Rio Grande River over time [ten Brink *et al.*, 2009]. Assuming the mass wasting occurred in a single event, the volume is estimated in ~ 26.7 Km^3 with an area of ~ 519.52 Km^2 and an excavation depth of ~ 160 m (from shelf to base of headwall scarp). The uppermost part of the sediment mass lies at an approximate water depth of 140 m. Figure 7 shows the bathymetry of the GOM's northwest corner that surrounds the East-Breaks scarp. Transect A-A indicates the location of the cross section used by both models, the simplified 3-D NS model and the commercial CFD code. As can be seen from Figure 7, transect A-A bisects the East-Breaks scarp in the direction of the mass wasting propagation. The resulting mass wasting along the transect is approximately 150 m thick (in average), 30 Km long and slides over a slope of $\sim 1.6\%$.

[42] On both numerical models, the 2-D domain size is 100 Km long \times 1.24 Km high. The domain has $1000 \times 2 \times$

124 cells, for a total of 496,000 cells. The two cells along the y direction arises from the channel domain configuration. The models spatial step or cell size (horizontal \times vertical) is 100×10 m (grid aspect ratio of 10). The water and mudslide densities are 1000 Kg/m^3 and 2000 Kg/m^3 , respectively. The inviscid-flow assumption is applied, this implies that viscous-shear and viscous-normal stresses are negligible, i.e., $\mu_1/\rho_1 = \mu_2/\rho_2 = 0$. Under the assumption of inviscid-flow, maximum energy transfer from the heavier fluid (mudslide) to the lighter fluid (water) is obtained during the mass wasting downslope acceleration. In effect, the boundary layer on the mudslide-water interface is neglected by this assumption too. This indicates that the boundary layer is very thin compared to the scale of the problem and it is believed that the absence of this boundary layer has a negligible effect relative to the modification of the landslide geometry as seen by the flow. As a result, the only stresses acting on the mudslide-water system is the normal stresses due to pressure. The chosen domain size has been tested for resolution sensitivity by increasingly refining the domain size and time step. The sequence of sensitivity tests reached a reasonable model solution or a convergent “true-value” approaching the previous value by less than 5%. The sequence of free surface and mudslide-water interface elevations derived from both models results are shown side by side in Figure 8.

[43] The diffusion of the mudslide material into the water column due to the low resolution required for efficient tsunami simulation is evident in the results of the commercial CFD model. As it is observed, the approach diffuses the mudslide material quite high in the water column. On the other hand, the simplified 3-D NS model

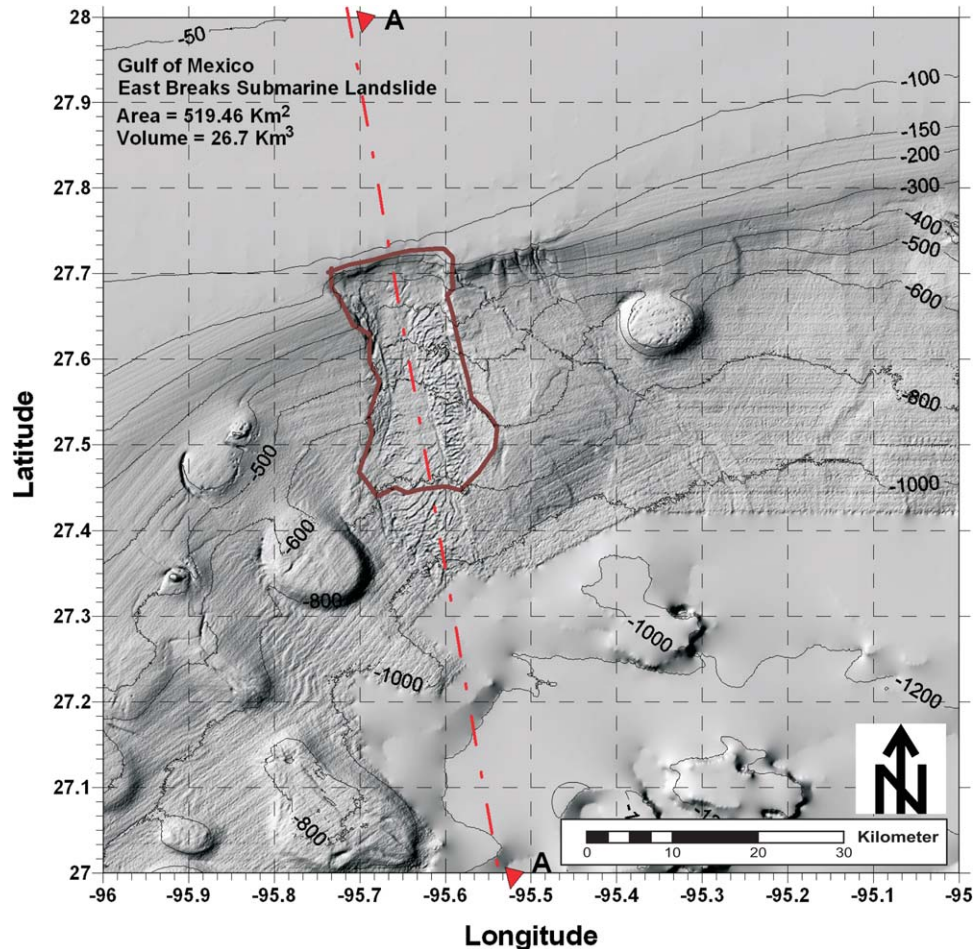


Figure 7. Scarp location and bathymetry of the GOM's East-Breaks underwater landslide. Transect A-A indicates cross-section used in the numerical model experiment setup for both numerical models, the simplified 3-D NS and the commercial CFD. Bathymetry is given in meters.

approach features ripples on the water-mudslide interface which are product of two-layers with different physical properties, named Kelvin-Helmholtz instability [Chandrasekhar, 1961]. In this particular case, the Kelvin-Helmholtz instability causes the free surface of the mudslide material to change into high-frequency components due to the sharp gradient of density and velocity, Gisler [2006] and the imposed condition to keep a sharp interface between the mudslide material and water, which is not allowed to roll up (packing method) [Nichols *et al.*, 1980]. Nevertheless, the free surface evolution obtained by both methods matched very well, see Figure 9. Several important observations are derived from the experiment. The initial tsunami wave configuration is mainly controlled by the early landslide kinematics and characteristics (initial slide acceleration, shape/volume, slope, etc.) and not by the subsequent slide deformation in deeper water. As the mudslide reaches deeper water, the effects of the mudslide deformation only cause minor changes to the main tsunami characteristics. Similar conclusion has been reported by Haugen *et al.* [2005], Grilli and Watts [2005], and Watts *et al.* [2005]. Therefore for this particular full-scale case, it seems that selecting either a sharp or a diffusive water-mudslide interface does not extremely affect the outcome

of the generated waves. It is noteworthy that the landslide generated waves usually have strong lateral spreading because as the waves radiate outward, their heights drop considerably. Lateral confinement in numerical or laboratory wave flume experiments (2-D) will produce larger wave amplitude and as a consequence faster waves, because the side-walls restraint the wave spreading. From previous submarine landslide studies, e.g., Gisler [2006] and Abadie *et al.* [2010], less viscous mudslides also produce longer mudslide runouts, leaving large deposit areas often enlarger by the diffusion process of the mudslide material into water. This reasoning implies that mudslides with a sharp interface will propagate slightly faster and probably will generate slightly large rebound waves at early stage of wave generation as can be seen from Figure 9.

[44] Following, a full-scale 3-D numerical simulation was carried out by using the simplified 3-D NS model to calculate the initial tsunami wave source generated by the East-Breaks underwater landslide. The wasting volume of $\sim 26.7 \text{ Km}^3$ used in this experiment is slightly larger than the one reported in ten Brink *et al.* [2009] of 21.95 Km^3 . The discrepancy is attributed to the different method used for the calculation of the volume. The volume was

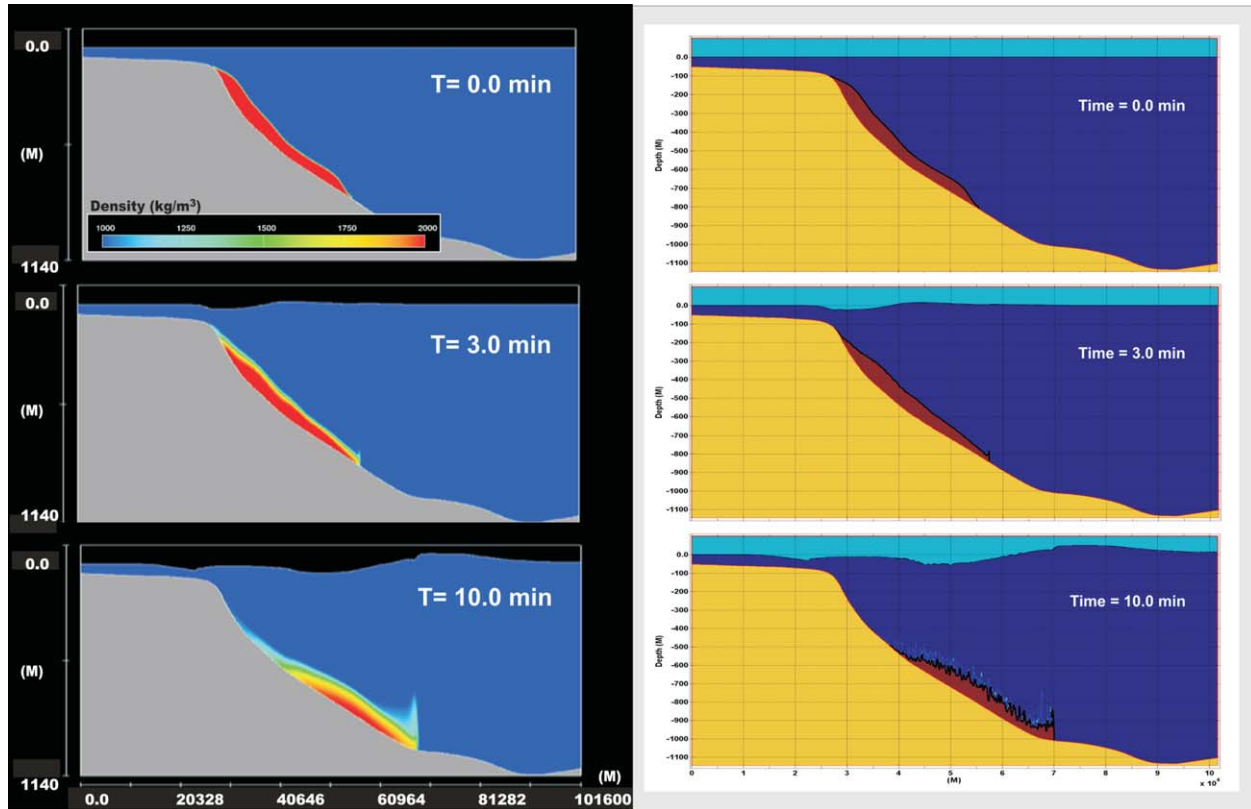


Figure 8. Side by side comparison of the free water surface and mudslide-water interface evolution for the 2-D East-Breaks underwater landslide numerical experiment along transect A-A (see Figure 7). (left) Diffusive interface results by the commercial CFD model; (right) sharp interface results by the simplified 3-D NS model results.

calculated by projecting tangentially the existing immediate isobaths located at the edges of the scarp to create smooth surfaces between the projected isobaths, gridding these smooth surfaces, and subtracting these surfaces from the gridded bathymetry of the scarp. On the other hand, the landslide volume reported by *ten Brink et al.* [2009] was calculated by interpolating smooth surfaces through polygons that define the edges of the slide [*ten Brink et al.*, 2006]. The 3-D domain dimension is 1×1 arc-degree² and 1.5 Km high. At latitude of ~ 27.5 arc-degree, the horizontal dimension of the domain is approximately 81.1 Km

long in the East-West direction and 111.3 Km long in the South-North direction. The domain grid resolution is $192 \times 240 \times 125$ cells, in the x , y , and z direction respectively, for a total of 5.76 millions cells. Thus, model's horizontal spatial steps are 422×464 m (x , y) and the vertical spatial step is variable ranging from 4 m to 16 m. The finer vertical resolution was confined in the water free surface and water-mudslide interface regions, in contrast with the coarser vertical resolution which was confined in the deeper water regions. The time steps was variable with a minimum value of 0.5 s. Viscosity coefficients μ_1/ρ_1 and μ_2/ρ_2 have been

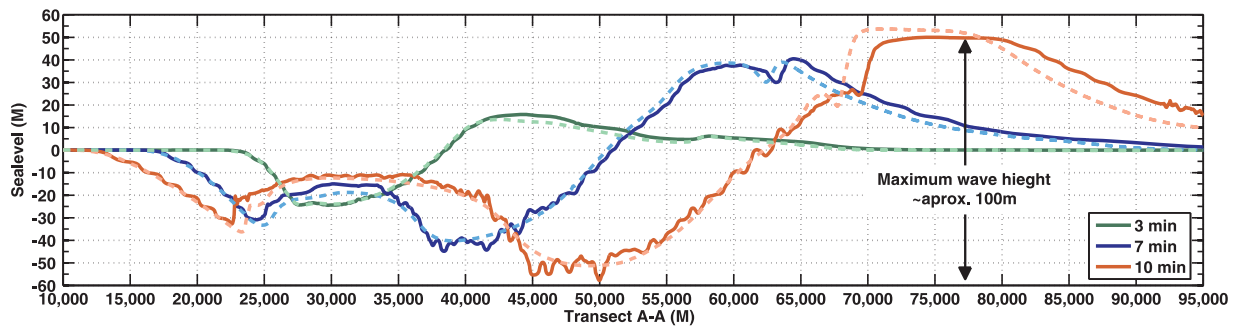


Figure 9. Snapshot of the free surface for the 2-D East-Breaks underwater landslide along transect A-A taken at time $t=[3, 7, 10]$ min. Free surface elevation comparison: commercial CFD model, broken line; simplified 3-D NS model, Solid line.

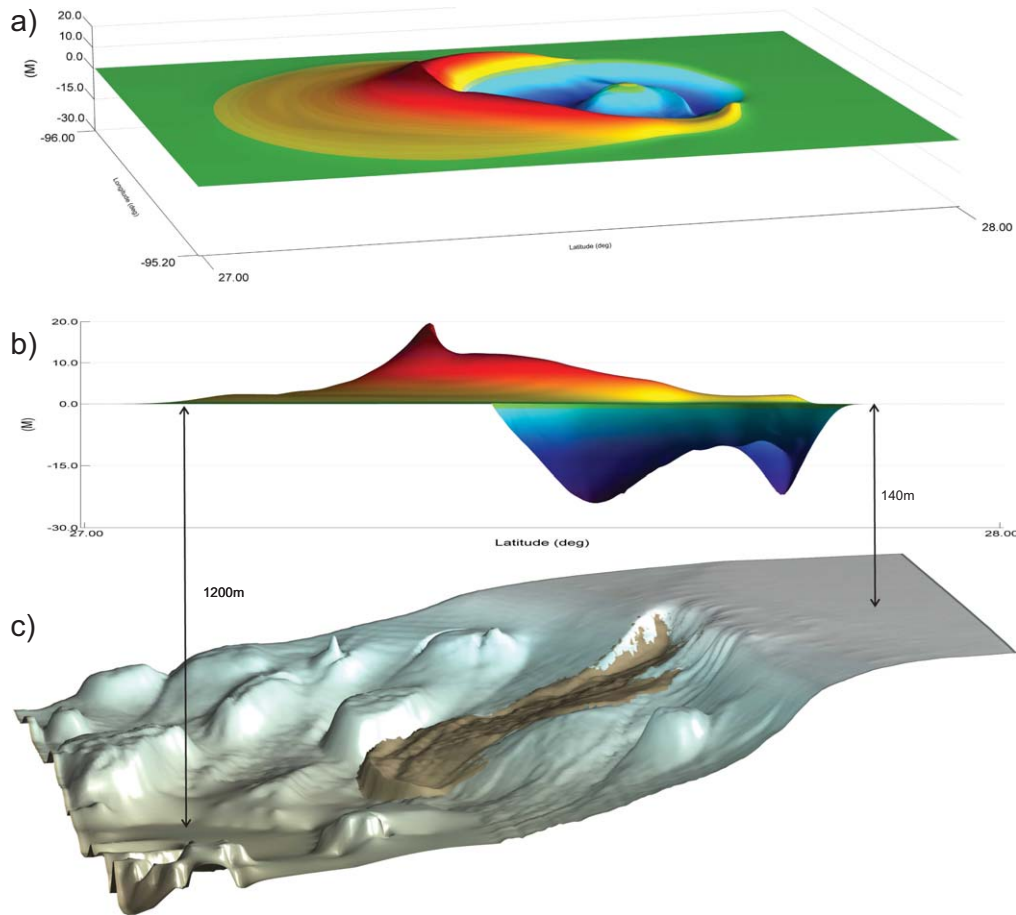


Figure 10. Simplified 3-D NS numerical results for the East-Breaks underwater landslide: (a) snapshot in perspective of the free surface at time $t = 10$ min, (b) snapshot of the wave profile at maximum wave height (time $t = \sim 7$ min), and (c) snapshot of the underwater landslide at time $t = 7$ min.

set to $1 \times 10^{-5} \text{ m}^2/\text{sec}$ to obtain a trade-off between maximum energy transfer during the mudslide downslope acceleration and numerical stability. The free slip condition was applied in all fluid cells neighboring a seabottom cell, i.e., $\partial \mathbf{u} / \partial z = 0$. Computer time required to simulate 10 min of the East-Break underwater landslide was ~ 24 h using a PC with 8 CPUs. Figure 10 depicts the simplified 3-D NS model's results for the determination of East-Breaks' initial tsunami wave source. As can be seen from the figure, the maximum generated wave height (~ 44 m) is recorded after 7 min of the slide initiation. The outgoing positive wave with amplitude of ~ 20 m is followed by a negative wave or initial surface depression of ~ 24 m caused by the underwater landslide down slope motion. Note that a rebounding wave is emerging from the surface depression between the outgoing and the negative back-going wave. The rebounding wave does not evolve as a massive wave, instead, as a short and dispersive wave, which is believed to be a consequence of the landslide motion in the subcritical regime $F_R = U_m / \sqrt{gD} \ll 1$; where U_m is the averaged mudslide velocity, D is the total water depth, and g is the gravitational acceleration.

[45] This initial tsunami source or wave is used for practical tsunami calculation for the construction of inundation maps along the GOM [Horrillo *et al.*, 2010]. A

common approach is to combine the 3-D model for the landslide-induced waves and a 2-D depth integrated non-hydrostatic or Boussinesq model for the wave propagation and runup (coupled model). The 3-D model provides the kinematic and the free surface configuration for the initial tsunami wave source, which is then inputted as the initial condition (hot start) to the more numerically efficient 2-D model for the calculations of the wave propagation and runup.

6. Conclusions

[46] In this study, a simplified three-Dimensional Navier-Stokes (3-D NS) model for two fluids (water-mudslide) is presented and validated by using a standard tsunami benchmark problem described in Liu *et al.* [2005] and Synolakis *et al.* [2007]. The simplification is derived from the large aspect ratio of the tsunami waves (wavelength/wave-height) and the selected computational grid that has a smaller aspect ratio. Based on the large aspect ratio of the wave and grid, a simplified surface height method is implemented. The fluid interfaces are assumed to be mostly horizontal in each individual free surface or water-mudslide interface cells. The sea level and mudslide interfaces are calculated based on the Volume of Fluid (VOF) function F

by integrating the fluxes of each individual fluid cell column wise. The donor-acceptor approach which prevents overflowing or over-emptying computational fluid cells in the advection process is simplified by only performing the over-emptying check for the donor cells. The pressure term has been split into two components, hydrostatic and nonhydrostatic. A hydrostatic solution can be obtained by merely switching off the second step of the projection method, which reduces the overall solution to a depth integrated approximation. The turbulence process is solved in a very simple manner using DNS or by adjusting the viscosity coefficient.

[47] Despite the simplification, an efficient solution is obtained. In general, the numerical results agree fairly well with the standard tsunami benchmark problem described in Liu *et al.* [2005] and Synolakis *et al.* [2007]. However, some small discrepancies in timing are evident, specifically, in the runup results. The rebound wave resulting from the drag of the landslide wedge is in general slightly overestimated by the model. The small difference is mainly attributed to the simplification of the model which does not resolve energy loss at the small-scale of the transient turbulence process. Even though the turbulence mechanism is solved at the grid scale in a very simple manner using DNS or by adjusting the viscosity coefficient value, the overall solution is adequate. Other contribution to the small difference in the overall solution, specially at the later time of the wave evolution, is attributed to the numerical friction. This arises mainly from the chosen discrete approximation of the momentum advection and to some extent to the numerical smoothing caused by the spatial and time resolutions. The effect on numerical results by using a sharp versus a diffusive water-mudslide interface for a full-scale tsunami landslide scenario was investigated. A 2-D numerical experiment with x , z (horizontal and vertical) axes was carried out using the simplified 3-D NS model and compared with a commercial CFD model, FLOW3D. Some important observations derived from the numerical experiment are as follows: (a) choosing a sharp or diffusive interface seems to have no remarkable effect on the size of the wave at early stage of the propagation. However, using a diffusive interface between the fluids will result in a slightly smaller and slower wave; (b) the tsunami initial wave evolution is mainly controlled by the early landslide kinematic characteristic (initial slide acceleration, shape/volume, and slope) and not by the posterior slide deformation. By the time such a deformation occurs, the slide would have reached deeper water and its effects on the tsunami characteristics become insignificant, see also Grilli *et al.* [2009].

[48] A full-scale 3-D numerical simulation was carried out by using the simplified 3-D NS model to calculate the initial tsunami wave source generated by the East-Breaks underwater landslide located in the GOM. The maximum generated wave height (~ 44 m) is recorded after 7 min of the slide initiation. The outgoing positive wave with amplitude of ~ 20 m is followed by a negative wave or initial surface depression of ~ 24 m caused by the underwater landslide down slope motion. A rebounding wave emerges from the surface depression between the outgoing and the negative back-going wave. The rebounding wave does not evolve as a massive wave, instead as a short and dispersive

wave, which is believed to be a consequence of the landslide motion in the subcritical regime. The simplified 3-D NS model performed fairly efficiently for underwater landslide domain sizes of the order of 6 million cells. Computer time required to simulate 10 min of landslide is around 24 h using 8 CPUs. The simplified 3-D NS model is able to handle relatively high resolution but obviously with high-computational cost.

[49] As it is recognized by the tsunami research community, the validation of numerical models is a continuous process. New laboratory experiments have continuously advanced to address new tsunami source characteristics. Future recommendations for additional landslide-tsunami testing are anticipated for the validation of the 3-D simplified model: e.g., like the rigid landslide described in Enet and Grilli [2007] and the deformable landslide described in Mohammed and Fritz [2012].

[50] **Acknowledgments.** The study has been funded by the National Tsunami Hazard Mitigation Program under award NA09NWS4670006, Construction of inundation maps in the Gulf of Mexico.

References

- Abadie, S. D., S. D. Morichon, S. Grilli, and S. Glockner (2008), VOF/Navier-Stokes numerical modeling of surface waves generated by subaerial landslides, *La Houille Blanche*, 1, 21–26.
- Abadie, S. D., S. D. Morichon, S. Grilli, and S. Glockner (2010), Numerical simulation of waves generated by landslides using a multiple-fluid Navier-Stokes model, *Coastal Eng.*, 57, 779–794.
- Assier-Rzadkiewicz, S., C. Mariotti, and P. Heinrich (1977), Numerical simulation of submarine landslides and their hydraulic effects, *J. Waterw. Port Coastal Ocean Eng.*, 123(4), 149–158.
- Campbell, C. S., P. W. Cleary, and M. Hopkins (1995), Large-scale landslide simulations: Global deformation, velocities and basal friction, *J. Geophys. Res.*, 100(B5), 8267–8283, doi:10.1029/94JB00937.
- Casulli, V., and G. S. Stelling (1998), Numerical simulation of 3D quasihydrostatic, free-surface flows, *J. Hydraul. Eng.*, 124, 678–686.
- Chandrasekhar, S. (1961), *Hydrodynamic and Hydromagnetic Stability*, Oxford Univ. Press, London.
- Chorin, A. J. (1968), Numerical solution of the Navier-Stokes equations, *Math. Comput.*, 22, 745–762.
- Clague, J. J., A. Munro, and T. S. Murty (2003), Tsunami hazard and risk in Canada, *Nat. Hazards*, 28, 433–461.
- Cranford, G. (2000), *Tidal Wave, A List of Victims and Survivors, Newfoundland, 1929*, pp. 264, Flanker Press, St. Johns, Newfoundland.
- Dellinger, J. A., and J. A. Blum (2009), Insights into the mechanism of the Northern Gulf of Mexico MS 5.3 “Green Canyon event” of 10 February 2006, AGU Fall Meeting Abstracts, p. A1484.
- Didenkulova, I., I. Nikolkina, E. Pelinovsky, and N. Zahibo (2010), Tsunami waves generated by submarine landslides of variable volume: analytical solutions for a basin of variable depth, *Nat. Hazards Earth Syst. Sci.*, 10, 2407–2419.
- Dunbar, P. K., and C. S. Weaver (2008), U.S. states and territories national tsunami hazard assessment: Historic record and sources for waves, Tech. Rep. to National Tsunami Hazard Mitigation Program, NGDC, U.S. Geol. Surv.
- Enet, F., and S. T. Grilli (2005), Laboratory experiments for tsunamis generated by underwater landslides: Comparison with numerical modeling, in *Proceedings of the 5th International on Ocean Wave Measurement and Analysis, IAHR Publ. paper 88*, p. 10.
- Enet, F., and S. T. Grilli (2007), Experimental study of tsunami generation by three-dimensional rigid underwater landslides, *J. Waterw. Port Coastal Ocean Eng.*, 133(6), 442–454.
- Enet, F., S. T. Grilli, and P. Watts (2003), Laboratory experiments for tsunamis generated by underwater landslides: Comparison with numerical modeling, in *Proceedings of the 13th International Offshore and Polar Engineering Conference, ISOPE03*, pp. 372–379, Honolulu, Hawaii.
- Fine, I. V., A. B. Rabinovich, E. A. Kulikov, R. E. Thomson, and B. D. Bornhold (1998), Numerical modelling of landslide generated tsunamis

- with application to the Skagway Harbor tsunami of November 3, 1994, paper presented at the International Conference on Tsunamis, Paris, pp. 211–223.
- Fritz, H. M. (2002), Initial phase of landslide generated impulse waves, PhD thesis Nr. 14'871, Swiss Federal Inst. of Technology (ETH), Zürich.
- Fritz, H. M., W. H. Hager, and H.-E. Minor (2003a), Landslide generated impulse waves: part 1: Instantaneous flow fields, *Exp. Fluids*, 35, 505–519.
- Fritz, H. M., W. H. Hager, and H.-E. Minor (2003b), Landslide generated impulse waves: part 2: Hydrodynamic impact craters, *Exp. Fluids*, 35, 520–532.
- Fritz, H. M., W. H. Hager, and H.-E. Minor (2004), Near field characteristics of landslide generated impulse waves, *J. Waterw. Port Coastal Ocean Eng.*, 139(6), 287–302.
- Fritz, H. M., F. Mohammed, and J. Yoo (2009), Lituya Bay landslide impact generated mega-tsunami 50th anniversary, *Pure Appl. Geophys.*, 166(1–2), 153–175, doi:10.1007/s00024-008-0435-4.
- Fritz, H. M., J. V. Hillaire, E. Molière, Y. Wei, and F. Mohammed (2013), Twin tsunamis triggered by the 12 January 2010 Haiti earthquake, *Pure Appl. Geophys.*, 170(9–10), 1463–1474, doi:10.1007/s00024-012-0479-3.
- Geist, E. L. (2000), Origin of the 17 July 1998 Papua New Guinea Tsunami: Earthquake or landslide?, *Seismol. Res. Lett.*, 71, 344–351.
- Gelfenbaum, G., and J. D. Smith (1986), Experimental evaluation of a generalized suspended sediment transport theory, in *Shelf Sands and Sandstones. Memoir*, edited by R. J. Knight and J. R. McLean, vol. 11, Can. Soc. of Pet. Geol., pp. 133–144.
- Gisler, G. (2006), SAGE calculations of the tsunami threat from La Palma, *Sci. Tsunami Hazards*, 24(4), 288–301.
- Gisler, G., R. Weaver, C. Mader, and M. Gittings (2004), Two- and three-dimensional asteroid impact simulations, *Comput. Sci. Eng.*, 6(3), 46–55, doi:10.1109/MCISE.2004.1289308.
- Gittings, M. L. (1992), SAIC's adaptive grid eulerian code, Defense Nuclear Agency Numerical Method Symposium, April 28–30, SRI International, Menlo Park, Calif.
- Grilli, S. T., and P. Watts (1999), Modelling of waves generated by a moving submerged body: Applications to underwater landslides, *Eng. Anal. Boundary Elements*, 23(8), 645–656.
- Grilli, S. T., and P. Watts (2005), Tsunami generation by submarine mass failure part I: Modeling, experimental validation, and sensitivity analyses, *J. Waterw. Port Coastal Ocean Eng.*, 131(6), 283–297.
- Grilli, S. T., S. Vogelmann, and P. Watts (2002), Development of a 3D numerical wave tank for modelling tsunami generation by underwater landslides, *Eng. Anal. Boundary Elements*, 26(4), 301–313.
- Grilli, S. T., O. S. Taylor, D. P. Baxter, and S. Marezki (2009), A probabilistic approach for determining submarine landslide tsunami hazard along the upper east coast of the united states, *Mar. Geol.*, 264, 74–97.
- Grilli, S. T., F. Dias, P. Guyenn, C. Fochesato, and F. Enet (2010), Progress in fully nonlinear potential flow modeling of 3D extreme ocean waves in Advances in Numerical Simulation of Nonlinear Water Waves (Series in Advances in Coastal and Ocean Engineering, Vol. 11, ISBN: 978–981-283-649-6), p. 55, World Scientific, Singapore.
- Hampton, M., and J. Locat (1996), Submarine landslides, *Rev. Geophys.*, 34, 33–59.
- Haugen, K. B., F. Lovholt, and C. B. Harbitz (2005), Fundamental mechanisms for tsunami generation by submarine mass flows in idealized geometries, *Mar. Pet. Geol.*, 22, 209–217.
- Heinrich, P. (1992), Nonlinear water waves generated by submarine and aerial landslides, *J. Waterw. Port Coastal Ocean Eng.*, 118(3), 249–266.
- Heinrich, P., A. Piatanesi, E. A. Okal, and H. Hébert (2000), Near-field modeling of the July 17, 1998 tsunami in Papua New Guinea, *Geophys. Res. Lett.*, 27, 3037–3040.
- Heinrich, P., A. Piatanesi, and H. Hébert (2001), Numerical modeling of tsunami generation and propagation from submarine slumps: The 1998 Papua New Guinea event, *Geophys. J. Int.*, 145, 97–111.
- Heller, V. (2007), Landslide generated impulse waves-prediction of near field characteristics, PhD thesis, Thesis dissertation presented to ETH Zurich, Zurich.
- Heller, V., and W. H. Hager (2010), Impulse product parameter in landslide generated impulse waves, *J. Waterw. Port Coastal Ocean Eng.*, 136(3), 145–155.
- Hirt, C. W., and B. D. Nichols (1981), Volume of fluid method for the dynamics of free boundaries, *J. Comput. Phys.*, 39, 201–225.
- Horrillo, J. (2006), Numerical method for tsunami calculation using full Navier-Stokes equations and volume of fluid method, PhD thesis, presented to the University of Alaska Fairbanks, 98 pp.
- Horrillo, J. J., A. L. Wood, C. Williams, A. Parambath, and G.-B. Kim (2010), Construction of tsunami inundation maps in the Gulf of Mexico, Tech. Rep. Award NA09NWS4670006, National Tsunami Hazard Mitigation Program (NTHMP), Natl. Weather Serv. Prog. Office, NOAA.
- Huber, A. (1980), Reservoir impulse waves caused by rockfall, Tech. Rep. Mitteilung 47, Lab. of Hydraul. Hydrol. and Glaciol., Swiss Federal Inst. of Technol.
- Huber, A. (1982), Impulse waves in Swiss lakes as a results of rock avalanches and bank slides. Experimental results for the prediction of the characteristic numbers of these waves, Commission Internationale des Grands Barrages, 14 Congres des Grand Barrages, Rio de Janeiro, pp. 311–390.
- Hunt, B. (1988), Water waves generated by distant landslides, *J. Hydraul. Res.*, 26, 307–322.
- Imamura, F., and K. Hashi (2002), Re-examination of the tsunami source of the 1998 Papua New Guinea Earthquake Tsunami, *Pure Appl. Geophys.*, 160, 2071–2086.
- Imamura, F., and M. A. Imteaz (1995), Long waves in two-layers: Governing equations and numerical model, *Tsunami Hazards*, 14, 13–28.
- Imteaz, M. A., and F. Imamura (2001), A non-linear numerical model for stratified tsunami waves and its application, *Sci. Tsunami Hazards*, 19, 150–159.
- Jiang, L., and P. H. Leblond (1992), The coupling of a submarine slide and the surface wave it generates, *J. Geophys. Res.*, 97(12), 731–744.
- Jiang, L., and P. H. Leblond (1993), Numerical modeling of an underwater bingham plastic mudslide and the wave which it generates, *J. Geophys. Res.*, 98, 304–317.
- Kawata, Y., et al. (1999), Tsunami in Papua New Guinea was as intense as first thought, *Eos Trans. AGU*, 80(101), 104–105.
- Kikuchi, M., Y. Yamanaka, Y. Abe, Y. Morita, and S. Watada (1998), Source rupture process of the Papua New Guinea Earthquake of July 17, 1998 inferred from teleseismic body waves, *Eos Trans. AGU*, 79(45), F573.
- Kowalik, Z., J. Horrillo, and E. Kornkven (2005a), Tsunami generation and runup due to 2D landslide, in *Advanced Numerical Models for Simulating Tsunami waves and Runup*, edited by H. Yeh, P. Liu, and C. Synolakis, pp. 269–272, World Scientific, Singapore.
- Kowalik, Z., J. Horrillo, and E. Kornkven (2005b), Tsunami runup onto a plane beach, in *Advanced Numerical Models for Simulating Tsunami waves and Runup*, edited by H. Yeh, P. Liu, and C. Synolakis, pp. 231–236, World Scientific, Singapore.
- Law, L., and A. Brebner (1968), On water waves generated by landslide, *Paper 2561 3rd Australas. Conference on Hydraulics and Fluid Mechanics*, pp. 155–159, Inst. of Eng., Sydney, Australia.
- Liu, P. L.-F., P. Lynett, and C. E. Synolakis (2003), Analytical solution for force long waves on a sloping beach, *J. Fluid Mech.*, 478, 101–109.
- Liu, P. L.-F., T. R. Wu, F. Raichlen, C. E. Synolakis, and J. C. Borrero (2005), Run-up and rundown generated by three-dimensional sliding masses, *J. Fluid Mech.*, 536, 107–144.
- Locat, J., and H. J. Lee (2002), Submarine landslides: Advances and challenges, *Can. Geotech. J.*, 39, 193–212.
- Lynett, P., and P. L.-F. Liu (2005), A numerical study of the run-up generated by three dimensional landslides, *J. Geophys. Res.*, 110, C03006, doi:10.1029/2004JC002443.
- Mader, C., and M. L. Gittings (2002), Modeling the 1958 Lituya Bay mega-tsunami, II, *Sci. Tsunami Hazards*, 20(5), 241–250.
- Mader, C., and M. L. Gittings (2003), Dynamics of water cavity generation, *Sci. Tsunami Hazards*, 21(2), 91–101.
- Mason, D., C. Habitz, R. Wynn, G. Pederson, and F. Lovholt (2006), Submarine landslides: Processes, triggers and hazard protection, *Philos. Trans. R. Soc. A*, 364, 2009–2039.
- Mohammed, F., and H. M. Fritz (2012), Physical modeling of tsunamis generated by three-dimensional deformable granular landslides, *J. Geophys. Res.*, 117, C11015, doi:10.1029/2011JC007850.
- Nichols, B. D., C. W. Hirt, and R. S. Hotchkiss (1980), SOLA-VOF: A solution algorithm for transient fluid flow with multiple free boundaries, *Tech. Rep. LA-8355*, Los Alamos Natl. Lab.
- Noda, E. K. (1970), Water waves generated by landslides, *J. Waterw. Harbors Coastal Eng. Div. Am. Soc. Civ. Eng.*, 96(WW4), 835–855.
- Novikova, L. E., and L. A. Ostrovsky (1978), Excitation of tsunami waves by a travelling displacement of the ocean bottom, *Mar. Geod.*, 2, 365–380.

- National Tsunami Hazard Mitigation Program (NTHMP) (2012), Proceedings and Results of the 2011 NTHMP Model Benchmarking Workshop, NOAA Spec. Rep., p. 436, U.S. Dep. of Comm./NOAA/NTHMP, Boulder, Colo.
- Okal, E. O., and C. E. Synolakis (2003), Theoretical comparisons of tsunamis from dislocations and slides, *Pure Appl. Geophys.*, *160*, 2177–2188.
- Pelinovsky, E., and A. Poplavsky (1997), Simplified model of tsunami generation by submarine landslides, *Phys. Chem. Earth*, *21*, 13–17.
- Pelinovsky, E. N. (2003), Analytical models of tsunami generation by submarine landslides, in *NATO Science Series*, edited by A. Yalciner et al., pp. 111–128, Earth Environ. Sci., 21, Kluwer, Dordrecht/Boston.
- Raichlen, F., and C. E. Synolakis (2003), Runup from three dimensional sliding mass, in *Proceedings of the Long Wave Symposium 2003*, edited by C. Briggs and M. Coutitas, pp. 247–256, XXX IAHR Congress Proc.
- Satake, K., and Y. Tanioka (2003), The July 1998 Papua New Guinea Earthquake: Mechanism and quantification of unusual tsunami generation, *Pure Appl. Geophys.*, *160*, 2087–2118.
- Shuto, N. (1991), Numerical simulation of tsunamis, in *Tsunami Hazard*, edited by E. Bernard, pp. 171–191, Kluwer Acad., Dordrecht, Netherlands.
- Sweet, S., E. Silver, H. Davies, T. Matsumoto, P. Watts, and C. Synolakis (1999), Seismic reflection images of the source region of the Papua New Guinea Tsunami of July 17, 1998, *Eos Trans. AGU*, *80*, F750.
- Synolakis, C. E., and F. Raichlen (2003), Waves and Runup generated by a three-dimensional sliding mass, in *Submarine Mass Movements and Their Consequences, Advances in Natural Hazards*, edited by J. Locat and J. Mienert, pp. 113–120, Kluwer Acad., Dordrecht.
- Synolakis, C. E., J.-P. Bardet, J. Borrero, H. Davies, E. Okal, E. Silver, S. Sweet, and D. R. Tappin (2002), Slump origin of the 1998 Papua New Guinea tsunami, *Proc. R. Soc. London, Ser. A*, *458*, 763–789.
- Synolakis, C. E., E. N. Bernard, V. V. Titov, U. Kanoglu, and F. I. Gonzalez (2007), OAR PMEL-135 standards, criteria, and procedures for NOAA evaluation of tsunami numerical models, Tech. Rep. NOAA Tech. Memo. OAR PMEL-135, NOAA/Pac. Mar. Environ. Lab., Seattle, Wash.
- Tanioka, Y. (1999), Analysis of the far-field tsunamis generated by the 1998 Papua New Guinea earthquake, *Geophys. Res. Lett.*, *26*, 3393–3396.
- Tanioka, Y., and L. J. Ruff (1998), The 1998 Papua New Guinea earthquake. An outer rise event?, *Eos Trans. AGU*, *79*, F572 (abstract).
- Tappin, D. R., P. Watts, G. M. McMurtry, Y. Lafoy, and T. Matsumoto (2001), The Sissano, Papua New Guinea Tsunami of July 1998—Off-shore evidence on the source mechanism, *Mar. Geol.*, *175*, 1–23.
- Tappin, D. R., P. Watts, and S. T. Grilli (2008), The Papua New Guinea Tsunami of 17 July 1998: Anatomy of a catastrophic event, *Nat. Hazards Earth Syst. Sci.*, *8*, 243–266.
- Tappin, D. R., et al. (1999), Sediment slump likely caused 1998 Papua New Guinea tsunami, *Eos Trans. AGU*, *80*(30), 329.
- ten Brink, U. S., E. L. Geist, and B. D. Andrews (2006), Size distribution of submarine landslides and its implication to tsunami hazard in Puerto Rico, *Geophys. Res. Lett.*, *33*, L11307, doi:10.1029/2006GL026125.
- ten Brink, U., D. Twichell, P. Lynett, E. Geist, J. Chaytor, H. Lee, B. Buczkowski, and C. Flores (2009), Regional assessment of tsunami potential in the Gulf of Mexico, Tech. Rep. NTHMP, U.S. Geol. Surv. Admin. Rep.
- Thomson, R. E., A. B. Rabinovich, E. A. Kulikov, I. V. Fine, and B. D. Bornhold (2001), On numerical simulation of the landslide-generated tsunami of November 3, 1994 in Skagway Harbor, Alaska, in *Tsunami Research at the End of a Critical Decade*, edited by G. Hebenstreit, pp. 243–282, Kluwer Acad., Dordrecht.
- Tinti, S., and E. Bortolucci (2000), Analytical investigation of tsunamis generated by submarine slides, *Ann. Geofis.*, *43*, 519–536.
- Tinti, S., E. Bortolucci, and C. Chiavettieri (2001), Tsunami excitation by submarine slides in shallow-water approximation, *Pure Appl. Geophys.*, *158*, 759–797.
- Titov, V. V., and C. E. Synolakis (1997), Extreme inundation flows during the Hokkaido-Nansei-Oki tsunami, *Geophys. Res. Lett.*, *24*(11), 1315–1318.
- Ward, S. N. (2001), Landslide tsunami, *J. Geophys. Res.*, *106*, 11,201–11,215.
- Watts, P. (1997), Water waves generated by underwater landslides, PhD thesis, Calif. Inst. of Technol., Pasadena, Calif.
- Watts, P. (1998), Wavemaker curves for tsunamis generated by underwater landslides, *J. Waterw. Port Coastal Ocean Eng.*, *124*(3), 127–137.
- Watts, P. (2000), Tsunami features of solid block underwater landslides, *J. Waterw. Port Coastal Ocean Eng.*, *126*(3), 144–152.
- Watts, P., S. T. Grilli, D. R. Tappin, and G. J. Fryer (2005), Tsunami generation by submarine mass failure. Part II: Predictive equations and case studies, *J. Waterw. Port Coastal Ocean Eng.*, *131*(6), 298–310.
- Wiegel, R. L. (1955), Laboratory studies of gravity waves generated by the movement of a submarine body, *Eos Trans. AGU*, *36*(5), 759–774.